The spatial-temporal patterns of Asian summer monsoon precipitation in response to Holocene insolation change: a model-data synthesis

Liya Jin [a, b, *], Birgit Schneider [b], Wonsun Park [c], Mojib Latif [c], Vyacheslav Khon [b], Xiaojian Zhang [a]

[a] *Key Laboratory of Western China's Environmental System, Research School of Arid Environment and Climate Change, Lanzhou University, Lanzhou 730000, China*

[b] *Institute of Geosciences, University of Kiel, Ludewig-Meyn-Str. 10, 24013 Kiel, Germany*

[c] *Helmholtz Zentrum für Ozeanforschung Kiel (GEOMAR), Duesternbrooker Weg 20, 24105 Kiel, Germany*

* Corresponding author. Tel.: +86 136 5945 5889; fax: +86 86 931 8912330

E-mail address: jinly@lzu.edu.cn (L. Jin)

To be submitted to

Quaternary Science Reviews

October 2013, revised manuscript

Abstract

Paleoclimate proxy records of precipitation/effective moisture show spatial-temporal inhomogeneous over Asian monsoon and monsoon marginal regions during the Holocene. To investigate the spatial differences and diverging temporal evolution over monsoonal Asia and monsoon marginal regions, we conduct a series of numerical experiments with an atmosphere-ocean-sea ice coupled climate model, the Kiel Climate Model (KCM), for the period of Holocene from 9.5 ka BP to present (0 ka BP). The simulations include two time-slice equilibrium experiments for early Holocene (9.5 ka BP) and present-day (0 ka BP), respectively and one transient simulation (HT) using a scheme for model acceleration regarding to the Earth's orbitally driven insolation forcing for the whole period of Holocene (from 9.5 to 0 ka BP). The simulated summer precipitation in the equilibrium experiments shows a tripole pattern over monsoonal Asia as depicted by the first modes of empirical orthogonal function (EOF1) of H0K and H9K. The transient simulation HT exhibits a wave train pattern in the summer precipitation across the Asian monsoon region associated with a gradually decreased trend in the strength of Asian summer monsoon, as a result of the response of Asian summer monsoon system to the Holocene orbitally-forced insolation change. Both the synthesis of multi-proxy records and model experiments confirm the regional dissimilarity of the Holocene optimum precipitation/effective moisture over the East Asian summer monsoon region, monsoon marginal region, and the westerly-dominated areas, suggesting the complex response of the regional climate systems to Holocene insolation change in association with the internal feedbacks within climate system, such as the air-sea interactions associated with the El Nino/Southern Oscillation (ENSO) and shift of the Intertropical Convergence Zone (ITCZ) in the evolution of Asian summer monsoon during the Holocene.

Keywords: Holocene; Asian summer monsoon; coupled climate model; orbital forcing

1. Introduction

Monsoon is a large-scale phenomenon of the seasonal cycle in various regions around the world and the associated precipitation changes are stronger in summer, i.e. June-July-August (JJA) over the Northern Hemisphere and December-January-February (DJF) over the Southern Hemisphere. Monsoon is also part of the global energetics and participates in the redistribution of heat and water across the two hemispheres as well as between land and ocean. Paleoclimate records and climate model simulations suggest that orbitally forced change in insolation was a major factor causing longer-term climate variations in the Holocene (e.g., Mitchell et al., 1988; Hewitt and Mitchell, 1998; Fleitmann et al., 2003, 2007; Mayewski et al., 2004; Gupta et al., 2005). Previous climate simulations (Weber et al., 2004) and proxy records (Staubwasser et al., 2003; Higginson and Altabet, 2004; Gupta et al., 2005; Selvaraj et al., 2007) have also shown that small (<1%) decadal to centennial scale solar irradiance can bring pronounced changes in the tropical monsoon during the Holocene. Accordingly, regional monsoon systems have undergone significant changes during the Holocene, and a common forcing mechanism (the Earth's orbital precession cycle) has been proposed to underlie low latitude climate dynamics acting synchronously on the different monsoon sub-systems (Beaufort et al., 2010). The Indian summer monsoon (ISM) and East Asian summer monsoon (EASM) are two sectors of the Asian summer monsoon systems, which are thought to be different from each other and also interactive with each other (Dao and Chen, 1957; Yeh et al., 1958). The East Asian summer monsoon climate during the Holocene associated with the summer precipitation in the monsoon influenced regions has been extensively studied in recent few decades with multiple climate models (e.g. Paleoclimate Modelling Intercomparison Project (PMIP) Mid-Holocene Climate Simulation, http://pmip.lsce.ipsl.fr/; Jiang et al., 2013) and various proxy records from cave deposits (speleothems), lake sediments (pollen, carbon isotopes of organic matter, total organic matter, stable isotopes of carbonates), peats (carbon isotopes of organic matter) and loess-paleosol sequences (grain size, magnetic susceptibility). Emerging empirical evidences suggest a decreasing trend of East Asian summer monsoon strength from the early Holocene (with the maximum monsoon intensity) to present day following the Northern summer insolation trend (Kutzbach, 1981; Ruddiman, 2008). However, dissimilarities have also been identified in the spatiotemporal patterns of the Asian summer monsoon during the Holocene. For example, a time-transgressive (asynchronous) Holocene climatic optimum was suggested that the Holocene East Asian summer monsoon precipitation (or effective moisture) reached the maximum at different periods in different regions of China with the trend of frontal migration paralleling the trend of Northern summer insolation across the monsoon region in a number of researches (An et al., 2000; He et al., 2004; Wang et al., 2010). A recent study by Jiang et al. (2012) suggested asynchronous termination of the Holocene climatic optimum in the Asian monsoon territory based on stalagmite-inferred precipitation in southwestern China. An anti-phase relationship is found in a few studies between the oxygen isotope records from stalagmites in caves in southern China and from loess/paleosol magnetic properties, the former indicating gradual monsoon weakening for the last 9 ka, while the latter indicating variable East Asian monsoon intensity through the entire Holocene (Hong et al., 2005; Dykoski et al., 2005; Maher and Hu, 2006; Maher, 2008). Multiple geochemical proxies (e.g. Organic carbon concentration (wt%), Organic carbon burial flux and C/N ratio) from the western Arabian Sea for the ISM strength, however, do not exhibit an inverse relationship with the EASM records, suggesting both the ISM and EASM varied in unison under common forcing factors on sub-Milankovitch timescales (Tiwari et al., 2005, and references therein). Tiwari et al. (2010) argued that during the Holocene, the ISM did not follow insolation, implying that there were more than one controlling factors than insolation (which declined monotonically) responsible for the monsoon strength and that other internal feedback process might be equally important. Recent work by Shi et al. (2012) suggested strong anti-phasing response of northern and southern East Asian summer precipitation to seasonal variability of the El Niño-Southern

Oscillation (ENSO) activity in a period of 20 ka in a long-term transient simulation.

The apparent inconsistences imply that the evolution history of Asian summer monsoon during the Holocene evidenced from paleoclimatic proxy records and confirmed with model simulations still have many controversies and uncertainties. The mechanisms that drive Asian summer monsoon at millennial-to centennial or longer time scales are still not fully understood. Therefore, more well-dated proxy records and climate modeling experiments as well as their comparison and further analyses are required for understanding the mechanisms behind the climate evolution of the Holocene. In this study, by using a coupled atmosphere-ocean-sea ice general circulation model (AOGCM), we performed a series of simulations of Holocene climate changes with varied orbital parameters, to investigate the mechanisms of Asian summer monsoon evolution and possible causes of asynchronous trends as some paleoclimate proxy data indicated in the two Asian sub-monsoon systems (i.e. the ISM and EASM). The outline of the paper is as follows. Section 2 briefly describes the climate model used in this study and the experimental setup. Section 3 displays the model results with a focus on the spatiotemporal patterns of summer precipitation in monsoonal and non-monsoon regions during the Holocene. Section 4 gives a comparison of simulated summer precipitation in sub-regions of China with multi-paleoclimate proxy records. A discussion is presented in Section 5 followed by the summary and concluding remarks in the final Section 6.

2. Methods

2.1. Model description

The coupled climate simulations discussed in this paper are performed with the Kiel Climate Model (KCM; Park et al., 2009), a non-flux-corrected coupled general circulation model, which consists of the atmospheric general circulation model ECHAM5 (Roeckner et al., 2003) and the Nucleus for European Modeling of the Ocean (NEMO) (Madec, 2008) ocean-sea ice general circulation model, with the

OASIS3 coupler (Valcke, 2006). The atmospheric resolution is T31 (3.75 °×3.75 °) horizontally with 19 vertical levels. The ocean horizontal resolution is on average 1.3 ° based on a 2 ° Mercator mesh, with enhanced meridional resolution of 0.5 ° in the equatorial region. The present-day climate simulated by KCM has been validated against the observation (Park et al., 2009) and used for the internal climate variability studies (Park and Latif, 2008, 2010) and externally forced variability (Latif et al., 2009). Schneider et al. (2010) showed the Holocene trends of the temperature simulated in a series of time-slice experiments with the KCM and provided in-depth analysis to explain the trends of the different proxy data in the Holocene. Khon et al. (2010) further presented the responses of the hydrological cycles simulated in the KCM. A detailed description of the KCM is given by Park et al. (2009) with further information of the performance of the model.

2.2. Experiment setup

First, we ran equilibrium simulations for two time slices using the KCM: the early Holocene (9.5ka BP, H9K) and the pre-Industrial (0 ka BP, H0K). The H9K and H0K experiments were both initialized with Levitus climatology data (Levitus, 1982) and were integrated 1000 years under the orbital configurations for the 9.5 ka BP and 0 ka BP, respectively. Greenhouse gas (GHG, i.e. the atmospheric concentrations of CO_2, CH_4 and N_2O) concentrations are held constant with pre-industrial levels. We analyze the last 500 years of the integrations after skipping initial 500 years to exclude model drifts.

Secondly, we performed a transient simulation (HT) for the period from the early Holocene (9.5 ka BP) to present day (0 ka BP). The transient simulation HT was started from the last year of the 1000-year equilibrium time-slice experiment H9K and is integrated under the orbital forcing for 1000 years after spin-up, thus the transient response of climate system during the Holocene (9.5 ka BP to 0 ka BP) is achieved. The Earth's orbital parameters (eccentricity, obliquity and precession; Berger and Loutre, 1991) are varied from 9.5 ka BP to 0 ka BP with a 10-times acceleration scheme (Lorenz and

Lohmann, 2004) in the HT simulation to save calculation resources. Since the variations in orbital parameters for the period of Holocene are very slow, the orbital accelerating effect for a factor of 10 can be neglected when considering the interannual-timescale changes of atmospheric and oceanic systems, such as the seasonal variability of paleo-ENSO in the model. GHGs were kept as constant as in the two time-slice simulations mentioned above and over the entire period of the transient Holocene simulation (from 9.5 to 0 ka BP). The three experiment setup is summarized in the Table 1.

Fig. 1 shows a comparison of model output from KCM simulation with observations of annual mean precipitation and surface temperature for 1901-1930 from the Climate Research Unit TS 2.1 climate dataset (Mitchell and Jones, 2005). The data quality of the observation during the periods can be questioned due to lack of the sampling, but the mean state at this period can be closer to the pre-industrial period that is simulated with the model. The spatial distribution and absolute values of simulated annual mean precipitation (Fig. 1c) and surface temperature (Fig. 1d) represent well the general features of the observations (Fig. 1a, b), in particular over the Indian and east Asian sectors. The same holds true for seasonal patterns (Figs. S1, S2, S3, S4).

It is to note here that the transient Holocene simulation (HT) by KCM has also made a comparison with 10 other climate modeling experiments in the Integrated Analysis of Interglacial Climate Dynamics Program (INTERDYNAMIK, http://www.geo.uni-bremen.de/Interdynamik/). The simulated trends of last 6 ka for global zonal-mean JJA precipitation and surface air temperature by KCM are in generally agreement with other models (Fig. S5), suggesting a reliable performance of KCM for the Holocene climate simulation.

2.3. EOF analysis

To investigate the spatial and temporal variations of Asian summer monsoon during the Holocene, the empirical orthogonal function (EOF) analysis (Björnsson and Venegas, 1997) was used in this study.

The EOF analysis is a novel statistical technique that simplifies an original spatial-temporal data set by transforming it into spatial patterns of variability and temporal projections of the patterns. The spatial patterns are the EOFs as basic functions in terms of variance. The associated temporal projections are the principal components (PCs) and are the temporal coefficients of the EOF patterns. Individual EOFs can sometimes have physical interpretation assigned to them. If there are geophysical data maps that are time series with any $m \times n$ matrix, Z, square or rectangular, there exist uniquely two orthogonal matrices, X and Y and diagonal matrix L such that,

$$Z = X \times L \times Y^{\mathrm{T}} \tag{1}$$

where Y^{T} is the transpose of a matrix Y. The columns of X called the EOFs of Z, and the corresponding diagonal elements of L are called the eigenvalues. Each row of Y serves as a series of time coefficients associated with each EOF, i.e. PC. The map associated with an EOF represents a pattern that is statistically independent and spatially orthogonal to the others. The eigenvalues indicates the amount of variance accounted for by the patterns.

In this study, Asian summer precipitation from the experiments H0K, H9K and HT by KCM, as a data set, respectively, constitutes a matrix Z, and is then performed with EOF analysis.

3. Model results

3.1. Surface temperature

Orbitally-induced changes in the seasonal distribution of insolation during the Holocene (Fig. 2) are clearly reflected by changes in surface temperature between simulations of H0K and H9K (Fig. 3). The zonally averaged northern Hemisphere insolation at 0 ka BP is over 30 W/m^2 lower than that at 9.5 ka BP in the middle and high latitudes during boreal summer (June) (Fig. 2). In response to the seasonal insolation changes, the simulated summer (June-July-August, JJA) surface temperatures in H0K shows a general cooling trend across most of the Eurasian continent relative to H9K, and extend to the northeastern EASM area (northeastern China, Korea and Japan) with maximum cooling, in excess of 2 °C (Fig. 3). The cooling in H0K compared to H9K is simulated north of 20 °N that extends from the Sahara in the northern Africa to 65 °N central Russia (Fig. 3). Surface temperatures over the ISM area (including India, southern and southwestern China), however, are warmer in H0K than H9K (Fig. 3). This warming trend over the ISM and southern EASM areas from 9.5 ka BP to 0 ka BP does not follow the summer (June) insolation evolution, which is gradually decreased during the Holocene (Fig. 2). The warming trend in summer surface temperature over the ISM and southern EASM regions, where is in contrast to the cooling trend over the middle and northern EASM regions, could be attributed to local effects related to a gradually decreasing summer monsoon cloud cover towards present day since early Holocene (Li and Morrill, 2010). Although a gradually decreasing summer insolation (Fig. 2) since the early Holocene tends to reduce the JJA surface temperature over the ISM and southern EASM regions, the decreasing cloud cover related to a weakening of the summer monsoon tends to increase the surface temperature over the ISM and southern EASM regions, which result in an asynchronous trends (from 9.5 ka BP to 0 ka BP) of surface temperatures during the Holocene in the ISM and EASM regions (Fig. 3).

3.2. Asian summer monsoon and associated precipitation

3.2.1. Summer monsoon intensity by index

Two Asian summer monsoon indexes (for the ISM and EASM regions, respectively) are calculated to indicate the strength and variability of the Asian summer monsoon. The Indian summer monsoon index (*ISMI*) used here is adapted from Goswami et al. (1999) as the difference of JJA meridional wind anomalies at 850 hPa and 200 hPa averaged over the ISM region, expressed as:

$$ISMI = V^*_{850} - V^*_{200} \qquad (2)$$

, where V^*_{850} and V^*_{200} are boreal summer (JJA) meridional wind anomalies at 850 hPa and 200 hPa respectively, averaged over the ISM region (70 º–110 ºE, 10 º–30 ºN).

The *EASMI* used here was defined as shear vorticity by Wang et al. (2008),

$$EASMI = U_{850}\,(110^{\circ}\text{–}140^{\circ}\text{E}, 22.5^{\circ}\text{–}32.5^{\circ}\text{N}) - U_{850}\,(90^{\circ}\text{–}130^{\circ}\text{E}, 5^{\circ}\text{–}15^{\circ}\text{N}) \quad (3)$$

, where U_{850} is boreal summer (JJA) horizontal wind speed at 850 hPa.

Both the *ISMI* and *EASMI* have been used extensively to indicate the intensity and variability of the Asian summer monsoon in modern climate change studies (e.g. Goswami et al., 1999, Wang et al., 2008). The Indian summer monsoon index, *ISMI*, in Eq. (2), proposed by Goswami et al. (1999) is based on the same dynamical premise as Webster and Yang Index (1992) that the monsoon flow is a first baroclinic response to the diabatic heating over southern Asia but with a better representation of the convective heating associated with the Indian summer monsoon precipitation. In addition, the *ISMI* in Eq. (2) is also a good measure of the strength of the monsoon Hadley circulation (Goswami et al., 1999). The All-India (India taken as one unit) monsoon rainfall has been used as a proxy data for Indian monsoon (Shukla and Paolino, 1983; Parthasarathy et al., 1994), but the *ISMI* represents much characteristics of the monsoon system (i.e., wind and rainfall) (Goswami et al., 1999). For the *EASMI*, Wang et al. (2008) once made a synthetic analysis on 25 existing EASM indices, and recommended a simple index of EASM intensity as shown in Eq. (3), which is nearly identical to a unified measure for the intensity of EASM, and has unique advantages over all the existing indices.

Fig. 4 depicts time series of the *ISMI* and *EASMI* derived from the transient Holocene simulation, HT. As can be seen in Fig.4, the *ISMI* indicates a generally declined trend of the Indian summer monsoon during the entire period of the Holocene (from 9.5 ka BP to 0 ka BP) (Fig. 4, black line), while the *EASMI* shows large oscillations of multi-centennial variability during mid-Holocene (roughly between 7 ka BP to 4.5 ka BP) (Fig. 4, red line), reflecting significant regional differences of the ISM and EASM, despite a similar overall decreased trend over the last 9.5 ka.

To further check the different regional evolution of Asian summer monsoon during the Holocene, we used an empirical orthogonal function (EOF) analysis (Björnsson and Venegas, 1997) on JJA precipitation in the following section.

3.2.2. Asian summer precipitation

EOF analysis is applied to summer (JJA) precipitation simulated in the experiments H0K, H9K and HT to provide the spatial structures and their time evolution. EOF modes from the time slice experiments with fixed orbital parameters (i.e. H0K and H9K) represent the internal variability of the precipitation that can be related to the monsoon system, while those from the transient simulations may provide the forced and internal variability as HT is forced by the varying orbital parameters.

The first EOF (EOF1) (Fig. 5a) derived from H9K JJA precipitation, which accounts for 18.77% of the total variance, depicts a tri-pole pattern with two significantly positive rainfall anomalies over the Indian subcontinent and the eastern EASM area including eastern China, Korea, most part of Japan and the adjacent marginal seas, respectively, and one negative rainfall anomalies in a broad corridor extending from Indochina Peninsula, crossing South China Sea and stretching to western North Pacific. The area with negative rainfall anomalies over western North Pacific was just described as the third sector of Asian-Pacific monsoon systems in modern climate (Wang and Lin, 2002). The associated time series of EOF1 (PC1) (Fig. 5b) shows a regular annual cycle. The EOF1 derived from H0K JJA precipitation (Fig. 5c) shows a quite similar spatial pattern with that derived from H9K (Fig. 5a), except that the explained variance of H0K JJA precipitation is slightly greater with 20.32% than that of 18.77% of H9K. The EOF1 derived from H9K and H0K JJA precipitation can be efficiently separated in the transient simulation, HT, as the second EOF mode (EOF2) (Fig. 5e) derived from HT JJA precipitation. Combining the patterns of EOF1 of H0K and H9K with their respective time series PC1 (Fig. 5b, d) and the pattern of EOF2 of HT with its time series PC2 (Fig. 5f), we see a distinct summer precipitation variation that could be attributed to the internal feedback processes within coupled monsoon systems over the ISM and EASM regions.

We next describe the forced mode obtained as the EOF1 derived from HT JJA precipitation, which accounts for 20.20% of the total variance. The EOF1 of HT JJA precipitation (Fig. 6a) shows a wave train pattern with significant negative rainfall anomalies extending from Peninsular India, crossing northern India along the foot of the Himalayas and stretching to northern China and southern Mongolia. The positive rainfall anomalies extending from the middle reaches of the Yangtze River Valley (100 º–122 ºE, 28 º–35 ºN) to Korea, Japan and adjacent marginal seas can also be observed in the EOF1 (Fig. 6a). Then, by combining the spatial pattern (EOF1) with associated time series (PC1) (Fig. 6b) of HT JJA precipitation, the spatial-temporal structure of the Asian summer monsoon precipitation can be described as follows. During the early to middle Holocene (from 9.5 to roughly 5.5-4.5 ka BP), a relatively high precipitation amount could be expected over the ISM influenced area (Indian sub-continent, northern India, Himalayas, southwestern China, northern China and southern Mongolia); while the precipitation over the eastern EASM influenced areas (Region D in China and Korea and Japan) is of the opposite phase. During the late Holocene (roughly from 5.5-4.5 ka BP to present), an inverse phase of precipitation amount could be expected over the above mentioned regions. The wave train pattern in EOF1 derived from HT JJA precipitation is on the millennial to centennial time scales, which is quite similar to a summer rainfall pattern in the semiarid region of northern China at the interannual and multidecadal time scales where teleconnection to the ENSO on summer rainfall in northern China through the Indian summer monsoon is suggested (Feng and Hu, 2004).

4. Comparison with paleoclimate proxy records

A great number of researches have been carried out on the history of Holocene climate changes over China from various proxy records including pollen and diatom assemblages, sediment lithology, lake levels, and geochemistry data in the past few years. The spatiotemporal changes of Holocene monsoon climate in China, especially the Holocene optimum in the monsoon region of China, have drawn much attentions to paleoclimatologists as it was not only an important recent climatic episode, it might as well be served as an important analog for future climatic change in a global warming background in the vast region. In this study, multi-proxy data, such as lake-level records, lacustrine and swamp deposits, fossil pollen sequences, peat bogs, speleothem cores and the magnetic susceptibility of loess-paleosol squences, were compiled for a measure or estimate of summer precipitation/effective moisture, or summer monsoon intensity during the Holocene in the regions where proxy record samples were collected. We concentrate on the period of Holocene optimum evaluated from model experiments and from proxy records. In order to show regional differences of changes in the simulated summer precipitation during the last 9.5 ka, we divide China into eight sub-regions (A-H) after An et al. (2000), based on physiography and model horizontal resolution used in this study (Fig. 7; Table 2). Table 2 lists the sites of proxy records in different regions with numbers 1-94. The sub-regions A, B, C, D, E, F, G and H in Table 2 match those in Fig. 7.

Region A is located in northwestern China, a vast area with extensively spreading of sandy deserts (e.g. Taklamakan Desert), where the climate is dominantly influenced by westerly winds. Region B is located at a transitional area that is both influenced by the westerly winds and monsoon front. In Region C (northeastern China), proxy data are from only few sites of lakes and swamps, peats, and pollen sequences (Table 2). Regions D (northern east-central China), E (southern east-central China), F (southeastern China), G (southwestern China), and H (southern Tibetan Plateau) are typical Asian summer monsoon influenced areas.

For Regions A, B, C, the entire desert belt in northern and northwestern China generally experienced a relatively wetter period from 8 to 4 ka BP (Yang et al., 2011) as evident from the synthesis of multi-paleoenvironmental records of geomorphologic, lacustrine, pedologic, geochemical, and faunal and floral fossil from China's Taklamakan (within Region A in Fig. 7), Badain Jaran Desert (within Region A in Fig. 7) and Hunshandake Sandy Lands (within Region B in Fig. 7). This is also generally consistent with the pollen and lake-level derived effective moisture records in western Inner Mongolia and Xinjiang (sites in Region A + some in Region B) supporting a relatively wetter period during 8.5-5.5 ka BP (Zhao et al., 2009a). A synthesis curve based mostly on pollen records across the monsoon margin region (the transitional zone between the East Asian summer monsoon and the westerly dominated region, covering most of proxy-record sites in region B, Fig. 7) shows the maximum moisture occurred during the middle Holocene (8-4 ka BP) (Zhao and Yu, 2012). In the summer monsoon influenced regions of China (Regions D, E, F, G, H and some areas in Regions C and A in Fig. 7), several synthesized analyses on the effective moisture index based on multi-proxy records for the Holocene yielded a generally consistent timing of the Holocene optimum during the period of 9.5-6 ka BP (e.g. Herzschuh, 2006; Zhao et al., 2009; Wang et al., 2010; Zhang et al., 2011).

Generally speaking, the period of the Holocene optimum was about during the early to middle Holocene (9-6 ka BP), based on the syntheses of multi-proxy data in the Asian summer monsoon region (Regions D, E, F, G, H + parts in Regions A, C) (Zhao et al., 2009a; Zhang et al., 2011); whereas in the westerly-dominated regions including the desert areas and monsoon marginal zone in northern China (Regions A, B, C), the timing of the Holocene optimum was about from 8 to 4 ka BP (Yang et al., 2011; Zhao et al., 2009b). The synthesis of vegetation indices for the monsoon margin region (as shown in Fig. 1 in work of Zhao and Yu, 2012, corresponding to region B in this study) as a whole shows that the maximum moisture occurred during the middle Holocene (8-4 ka BP) and the driest conditions during the late Holocene (4-0 ka BP) (Zhao and Yu, 2012), coinciding with the simulated summer precipitation (July, August) for region B (Fig. 8).

The described coupled AOGCM transient experiment (HT) reveals temporal response of summer precipitation to orbitally induced insolation forcing over the last 9.5 ka. The tripole spatial pattern of summer (JJA) precipitation seen in the first EOF mode (EOF1) of the HT experiment (Fig. 6) indicates regional difference within Asian monsoon regions. Time series of anomalies of boreal summer precipitation evaluated using model grid points that correspond as closely as possible to eight regions are compared with the syntheses of multi-proxy data given in Fig. 8. As can be seen from Fig. 8, the simulated maximum summer precipitation (positive anomalies) are similar in Regions A and B, occurred about 9-4.5 ka BP (July, A, B), 9-4.5ka BP (August, A) and 8.5-6 ka BP (August, B) respectively, while in Region C, the simulated maximum precipitation were about 7-3 ka BP (July, C) and 9.5- 4.5 ka BP (August, C), respectively. The simulated maximum summer precipitation in Regions A, B, C is in generally consistent (or overlapped) to the timing of the Holocene optimum from proxy-based moisture index (Zhao et al., 2009a; Yang et al., 2011) (Fig. 8). But it is noticed that in Regions A and B, the multi-proxy records showed a relatively drying period during 9.5-8.5 ka BP (Zhao et al., 2009a; Yang et al., 2011), while the simulated summer (July, August) precipitation over the regions is about positive normalies (Fig. 8). This may be due to the fact that in the mid-latitude westerly-dominant areas, like the arid central Asia (Chen et al., 2008) and the northwestern China (Region A), the dry conditions in the early Holocene seem to result mostly from changes in winter rather than summer climate (Jin et al., 2012). The simulated maximum summer (July, August) precipitation in the monsoon regions (Regions E, F, G) (Fig. 9) experienced a roughly synchronous period of rich rainfall (positive anomalies) at 9-5.5 ka BP, which can be comparable to the moisture index induced Holocene optimum period based on the syntheses of multi-proxy data for the period of Holocene (Zhao et al., 2009b; Zhang et al., 2011).

It is worthy to note that in Region H (southern Tibetan Plateau), a wetter period during 9.5 to 5.5 ka BP (with positive anomalies) was similar to that in regions E, F and G, but in the late half of the

Holocene (i.e. from 5.5 ka BP to present), the rapidly decreased trend of summer precipitation is quite different from that in Regions E, F and G (Fig. 9). This might be due to the result of Region G is much more influenced by the ISM than by EASM (compare with the *ISMI* in Fig. 4). Also in Region D (northern east-central China), we noticed an obvious reverse phase trend of summer (July, August) precipitation during 9.5 ka-5.5 ka BP, as compared with that in region E (southern east-central China) (Fig. 9). The distinct temporal patterns of the simulated summer precipitation during the last 9.5 ka between Region D (within the northern EASM region) and Region E (within the southern EASM region) is similar to a reverse phase relation between northern (105 º–150 ºE, 30 º–45 ºN) and southern (105 º–150 ºE, 15 º–30 ºN) East Asian summer monsoon precipitation found from the outputs of an orbital forcing-driven 284 ka long-term transient simulation (Shi et al., 2012).

5. Discussion

5.1. The role of orbital forcing

It has been widely accepted that the Earth's orbital forcing induced insolation changes play a central role in the global scale climate changes in the last 11.5 cal ka (Mayewski et al., 2004). This insolation driving mechanism on Holocene climate change is supported by climate modeling experiments of global monsoon variations (e.g. Kutzbach et al., 1982; Liu et al., 2004; Bosmans et al., 2012). These modeling experiments of monsoonal response to Holocene orbital forcing are mostly time-slice experiments for 9 ka BP (e.g. Kutzbach et al., 1982) or 6 ka BP (e.g. Joussaume et al. 1999) with the orbital parameters assigned to constant values at corresponding time (i.e. 9ka BP or 6 ka BP). In the present study, the orbital parameters are set varying along with time (from 9.5 ka BP to 0 ka BP) in the transient experiment HT, making it to allow for checking the entire Holocene course of the variations of the spatial patterns of summer precipitation.

The inhomogeneous distribution of summer precipitation in the Asian monsoon region in EOF 1 of

HT (Fig. 6a) implies the different response of the individual sub-regions of the Asian summer monsoon domain (i.e. the ISM and EASM) to the Holocene insolation change. The ISM is primarily characterized by meridional thermal contrast and pressure gradient between northern Asian continent and southern Indian Ocean, while the EASM is controlled by the zonal land-ocean thermal contrast and pressure gradient between the Asian continent and the western Pacific. Consequently, the Holocene insolation change has a different effect on the two sub-systems of ISM and EASM, as suggested by Dallmeyer et al. (2013) that the different response of the Indian and East Asian monsoon systems to the Holocene insolation forcing is due to their dynamical change in the different seasons.

The stronger boreal summer insolation during the early to middle Holocene compared to present-day is believed to have strengthened monsoon activity and accentuated the northerly bias of the Intertropical Convergence Zone (ITCZ) (e.g., Kutzbach, 1981; Koutavas et al., 2006). Accordingly, sites affected by the monsoons typically reflect positive precipitation anomalies during the early to middle Holocene, as evidenced by multi-proxy records in the Asian summer monsoon regions and simulated in the HT experiment (Figs. 8, 9). Previous researches have shown that tropical Pacific SST changes may have great influences on the East Asian monsoon system within ENSO cycles (e.g. Wang et al., 2000, 2003; Lau and Nath, 2006). Thus, a strong relationship was suggested to operate between the ITCZ position, tropical Pacific SSTs, and ENSO throughout the Holocene (e.g. Koutavas et al., 2006). To examine whether a tele-connection between Asian summer monsoon and Pacific existed or not during the Holocene, the correlation coefficient is calculated between PC1 of HT JJA precipitation (representing the Asian summer monsoon intensity) and ENSO index (representing ENSO variability) (Fig. 10). The ENSO index here is based on the Niño 3.4 SST from the 9.5 ka transient simulation (HT). It shows that the simulated ENSO variability (Fig. 10, red line) is quite well consistent with the Holocene ENSO frequency (Fig. 10, black line) inferred from Laguna Pallcacocha sediment color changes (Moy et al., 2002), with a relatively weak ENSO variability during the early Holocene (about 9-7 ka BP) and an increased variability during late Holocene (2.5-1.0 ka BP) (Fig. 10), which is also inferred from previous modeling experiment (Liu et al., 2000). The PC1 of HT JJA precipitation shows a stepwise increased trend during 9.5 ka BP to 0 ka BP with relative large century-scale variations during 2.5-1 ka BP (which is similar to that in ENSO variability) corresponding to gradually weakened summer monsoon precipitation as can be compared with the Holocene evolution of two sub-Asian summer monsoon systems (Fig. 4). The high correlation (R = 0.74) (Fig. 10) between the PC1 of the Asian summer precipitation and ENSO index during the last 9.5 ka suggests an important ENSO modulation in the millennial-centennial time-scales of orbital forcing, similar as the ENSO influence on interannual change in the East Asian summer precipitation (Wang et al., 2000) and in the precession scale East Asian summer monsoon variability from a long-term (284 ka) transient simulation using the fully-coupled fast ocean-atmosphere model (FOAM) (Shi et al., 2012).

The ITCZ is usually located over the warmest surface in association with high cloudiness, frequent thunderstorms and heavy rainfall. The position of the ITCZ can be represented by the variations of zonally averaged mean JJA outgoing longwave radiation (OLR) between 105 º–150 ºE. As is seen from Fig. 11, the gradually increased OLR (negative values mean upward radiation) along 20 ºN indicates a mean southward shift in the position of the ITCZ in the last 9.5 ka, which can be well compared with the runoff variability in the Ti record of the Cariaco Basin, a proxy indicator for the Pacific ITCZ in the Holocene (Haug et al., 2001). The general southward shift of the ITCZ over the course of the Holocene (Fig. 11) is accompanied by gradually weakened Asian summer monsoon (Fig. 4) and associated summer precipitation variations in monsoon regions (Figs. 8, 9). Since around 5 ka BP, there seemed to be a phase transition of the summer (July, August) precipitation anomalies from positive sign to negative in Regions E, F, G, H (Fig. 9), implying an increased coupling interaction between the enhanced ENSO variability (Fig. 10, red line) and southward ITCZ (Fig. 11, black line) with the smooth insolation forcing in the late Holocene (Fig. 2). The temporal trends in the Asian summer precipitation, ENSO variability, and the shifting ITCZ suggest that the potential of orbital forcing induced insolation to affect the Asian summer monsoon precipitation acts through its influence on the large annual cycle of SST, convection and cloud cover in the eastern tropical Pacific.

5.2. Holocene optimum in monsoonal Asia and marginal monsoon regions

As shown in Figs. 8, 9, the timing of Holocene optimum of summer precipitation appears to vary in different regions from various proxy records and model results. Most sites in the monsoon regions (E, F, G, H) show approximately consistent variations of peak summer precipitation or effective moisture at 9-6 ka BP (Fig. 9), suggesting that the Holocene optimum, defined by peak summer monsoon precipitation/effective moisture (An et al., 2000), occurred broadly synchronous and that the previously-proposed time-transgressive Holocene climate across China (e.g., An et al., 2000) is not supported by current study. The general comparability of Asian summer monsoon (Fig. 4) with the northern hemisphere summer insolation curve (Fig. 2) during the last 9.5 ka indicates that the orbitally induced insolation was a major controller on the variability of Asian summer monsoon during the Holocene, in spite of the fact that various climatic feedbacks within Asian summer monsoon system is of great importance, such as the effect of oceanic feedback (e.g. Liu et al., 2004). However, the appearance of the distinct spatial-temporal patterns in the simulated summer precipitation (Fig. 6a, Fig. 9) in the ISM area (Indian sub-continent, southwestern, southern China) (Regions F, G, H in Fig. 7) and northern east-central China (Region D in Fig. 7) reveals the complexity of the response of the Asian summer monsoon system to the Holocene insolation change. The simulated summer precipitation in the southern Tibetan Plateau (Region H), where is mainly influenced by the ISM, shows a rapidly decreased trend (a transition of precipitation from positive to negative) after about 5 ka BP (Fig. 9) that largely different from that in EASM influenced areas (Regions D, E). This further confirms that the variability of the ISM and EASM systems may not be synchronous due to different mechanism between the two monsoon domains.

The climate of Regions A, B, C (Fig. 7) is influenced by large-scale climate forcing, including the Asian monsoon (Indian monsoon, the East Asian monsoon) and the prevailing mid-latitude westerly winds (Chen et al., 2008). The timing of Holocene summer precipitation/moisture maximum during 8.5 to 4-5.5 ka BP evidenced by multi-proxy records (Yang and Scuderi, 2010; Yang et al., 2011) in most sites in Regions A and parts in B (including Xinjiang, the northwestern Loess Plateau, and western Inner Mongolia), where the westerly winds dominates, is to some extent later than that during 9-6 ka BP in the monsoon region (E, F, G, H) (Fig. 9), reflecting the difference in the response of regional climate to Holocene insolation change. The relatively dry period during 9.5-8.5 ka BP in most sites in Regions A and parts in B and further to the west in arid central Asia (Chen et al., 2008) is closely related to a reduction in moisture advection brought both by the weakening of mid-latitude westerly winds and decreased upstream evaporation, which is resulted from a reduced meridional temperature gradient forced by latitudinal differences in orbital forcing in the early Holocene compared to present day (Jin et al., 2012). In the Asian summer monsoon marginal region (corresponding to most sites in Region B), the simulated positive (negative) anomalies in summer precipitation during 9.5 to 5-6 ka BP (during 4.5-0 ka BP in July and 6-0 ka BP in August) (Fig. 8) are in general agreement with the synthesized vegetation indices of Maximum moisture (during 8-4 ka BP) and gradually drying conditions afterwards (Zhao and Yu, 2012), likely to reflect the northward extension of the Asian summer monsoon during the early- to middle Holocene and the retreat during the late Holocene in response to the insolation change during these periods.

5.3. Air-sea interactions

As discussed above, the spatial-temporal patterns in the Asian summer monsoon precipitation inconsistently responded to the Holocene insolation change. Here, we analyze the circulation pattern using HT experiment result to explain the different evolutions of the ISM and EASM and regional differences in the East Asian region. Fig. 12 shows the spatial pattern of composite differences of 850 hPa wind vectors and sea level pressure (SLP) over northern and tropical Pacific and adjacent continents between low- and high- DJF Niño SST extremes (ENSO events), where the low (high) SST extremes are corresponded to the low (high) frequency of ENSO events at early (late) Holocene (corresponding to 9-8 ka BP (2.5-1.5 ka BP) (Fig. 10). A high pressure center is over northwestern Pacific with an enhanced anticyclone activity, which delivers large water vapor from northwestern Pacific toward the northern China and southern Mongolia (Fig. 12), which is favorable for the development of East Asian summer monsoon and associated rainfall over there (Fig. 6a; some areas in Regions B, C in Fig. 7). Similar northward lower level winds (from ocean to land) can be seen over the sub-Indian continent and southeastern Asia (corresponding to Regions E, F, G, H), bringing large water vapor to the regions and hence plentiful rainfall (Fig. 6a).

The pronounced changes in the SLP over the northwestern Pacific (Fig. 12) are closely related to the SST changes over northwestern Pacific (Fig. 13). The negative SST anomalies (cooling) over the northwestern Pacific, lasting out from preceding winter (Fig. 13a) to the present summer (Fig. 13c) through the springtime (Fig. 13b), tends to induce an anomalous high pressure over the northwestern Pacific (Fig. 12), which in turn with an enhanced anticyclone strengthens southeasterly wind over East Asia and favors the development of East Asian summer monsoon as discussed above (Fig. 12). And then the displacement of the east-west oriented precipitation belt following the ITCZ north- and southward movement (Fig. 11) could be resulted from changes in the regional circulation due to the change in sea-land temperature difference (Figs. 12, 13).

6. Conclusions

A series of numerical experiments, including the Holocene transient simulation (HT) by using a method for model acceleration regarding to the Earth's orbitally driven insolation forcing and time slice simulations (H0K, H9K), were conducted with the coupled atmosphere-ocean-sea ice general circulation model, the Kiel Climate Model (KCM). Model results have been compared to synchronous multi-proxy records of precipitation/moisture for the monsoonal Asia and marginal monsoon regions. Overall the model results are generally comparable to the synthesis of the multi-proxy records. A tripole spatial structure and diverging trends of summer precipitation across the Asian monsoon region in the 9500 year-long transient simulation (HT) were revealed. According to the simulations by KCM, a relatively high precipitation prevailed over the ISM influenced area (Indian sub-continent, northern India, Himalayas, southwestern China, northern China and southern Mongolia) during the early to middle Holocene (from 9.5 to roughly 5.5-4.5 ka BP), which is closely related to the stronger Indian summer monsoon at that period than present day. The precipitation over the eastern EASM influenced areas (Region D in China, Korea and Japan) is of the opposite phase of that in the ISM influenced area, suggesting the different responses of the Indian and East Asian summer monsoon systems to the Holocene insolation forcing. In particular, the regional dissimilarities in the evolution of EASM precipitation during the Holocene (e.g. Regions D, E) imply that the response of the EASM to the Holocene insolation changes is in conjunction with internal feedbacks within climate system, such as the air-sea interactions associated with the ENSO and subsequent north/southward shifts in the position of the inter-tropical convergence zone (ITCZ).

The timing of Holocene summer precipitation/moisture maximum in northwestern and northern China (Regions A and B) was about during 8.5 to 4-5.5 ka BP, slightly later than that during 9-6 ka BP in the Asian summer monsoon region (E, F, G, H), reflecting the different response of rainfall changes in the mid-latitudinal westerly wind influenced areas (A, B) and EASM domain to the Holocene insolation change. This is closely related to the regional temperature change directly influenced by insolation change and associated reorganization of atmospheric circulation over Eurasia and EASM region.

An early Holocene (9-8 ka BP) drought epoch over westerly wind dominated region (A) inferred by proxy records was not resolved by model simulation, suggesting that further experiments including more possible impacting factors such as solar irradiance forcing on Holocene Asian climate changes are necessary to test the contribution of the insolation effect versus oceanic feedbacks through tele-connection with North Atlantic and Pacific Oceans as well as the changes in GHGs concentration to the Holocene Asian summer monsoon changes.

Acknowledgements This research was jointly supported by the National Basic Research Program of China (973 Program, Nr. 2010CB950202; Nr. 2010CB950204), the National Natural Science Foundation of China (NSFC, Nr 41275071; Nr. 41130102) and the Deutsche Forschungsgemeinschaft (DFG) supported Cluster of Excellence “The Future Ocean” (EXC 80/1). Sincere thanks are extended to four anonymous reviewers for their constructive comments and helpful suggestions for the earlier version of this paper. The KCM modeling experiments were performed at Kiel University’s computing center, which is also appreciated.

References

An, Chengbang, Feng, Zhaodong, Tang, Lingyu, 2003. Evidence of a humid mid-Holocene in the western part of the Chinese Loess Plateau. Chinese Science Bulletin 48, 2472–2479. (23B, 24B)

An, Z., Porter, S.C., Zhou, W., Lu, Y., Donahue, D., Head, J., Wu, X., Ren, J., 1993. Episode of strengthened summer monsoon climate of Younger Dryas age on the Loess Plateau of central China. Quaternary Research 39, 45–54. (20B)

An, Z., Porter, S.C., Kutzbach, J.E., Wu, X., Wang, S., Liu, X., Li, X., Zhou, W., 2000. Asynchronous Holocene optimum of the East Asian monsoon. Quaternary Science Reviews 19, 743–762.

Beaufort, L., van der Kaars, S., Bassinot, F.C., Moron, V., 2010. Past dynamics of the Australian monsoon: precession, phase and links to the global monsoon concept. Climate of the Past 6, 695–706.

Berger, A., Loutre, M.F., 1991. Insolation values for the climate of the last 10 million years. Quaternary Science Review 10 (4), 297–317.

Berkelhammer, M., Sinha, A., Stott, L., Cheng, H., Pausata, F.S.R., Yoshimura, K., 2012. An abrupt shift in the Indian monsoon 4000 years ago, in Climates, Landscapes, and Civilizations, Geophys. Monogr. Ser., vol. 198, edited by L. Giosan et al., 75–87, AGU, Washington, D. C., doi:10.1029/2012GM001207. (88H)

Björnsson, H., Venegas, S.A., 1997. A manual for EOF and SVD analyses of climate data. McGill University, CCGCR Report No. 97-1, Montréal, Québec, 52pp.

Bosmans, J.H.C., Drijfhout, S.S., Tuenter, E., Lourens, L.J., Hilgen, F. J., Weber, S. L., 2012. Monsoonal response to mid-holocene orbital forcing in a high resolution GCM. Climate of the Past 8, 723–740, 2012, doi:10.5194/cp-8-723-2012.

Cai, Y., Tan, L., Cheng, H., An, Z., Edwards, R.L., Kelly, M.J., Kong, X., Wang, X., 2010. The variation of summer monsoon precipitation in central China since the last deglaciation. Earth and Planetary Science Letters 291, 21-31. doi:10.1016/j.epsl.2009.12.039. (27B)

Chen, Fahu, Li, Jijun, Zhang, Weixin, Pan, Baotian, 1991a. The loess profile of south bank, climate information and lake-level fluctuation of Qinghai Lake during the Holocene. Scientia Geographica Sinica 11 (1), 76–85 (in Chinese). (13B)

Chen, F., Li, J., Zhang, W., 1991b. Loess stratigraphy of the Lanzhou profile and its comparison with deep-sea sediment and ice core record. GeoJournal 24 (2), 201–209. (18B)

Chen, F., Chen, B., Zhao, Y., Madsen, D., 2006. Holocene environ- mental change inferred from high-resolution pollen records from inland lake deposits, arid China. The Holocene 16, 675–684. (16B)

Chen, F., Yu, Z., Yang, M., Ito, E., Wang, S., Madsen, D.B., Huang, X., Zhao, Y., Sato, T., Birks, H.J.B., Boomer, I., Chen, J., An, C., Wünnemann, B., 2008. Holocene moisture evolution in arid central Asia and its out-of-phase relationship with Asian monsoon history. Quaternary Science Reviews 27, 351–364.

Chen, W., Wang, W.M., Dai, X.R., 2009. Holocene vegetation history with implication of human impact in the lake Chaohu area, Anhui Province, East China. Vegetation History and Archaeobotany 18, 137–146. (64E)

Cui, Zhijiu, Song, Changqing, 1992. The periglacial phenomenon and environmental evolution during Holocene in Daqingshan (mountain). Glacier and Permafrost 14, 325–331 (in Chinese). (35B, 39B)

Dallmeyer, A., Claussen, M., Wang, Y., Herzschuh, U., 2013. Spatial variability of Holocene changes in the annual precipitation pattern: a model-data synthesis for the Asian monsoon region. Climate Dynamics 40, 2919–2936, doi: 10.1007/s00382-012-1550-6.

Dao, Shih, Chen, Lungshun, 1957. The structure of general circulation over continent of Asia in summer. Acta Meteorologica Sinica 28 (3), 234–247 (in Chinese).

Dong, J., Wang, Y., Cheng, H., Hardt, B., Edwards, R.L., Kong, X., Wu, J., Chen, S., Liu, D., Jiang, X., Zhao, K., 2010. A high-resolution stalagmite record of the Holocene East Asian monsoon from Mt Shennongjia, central China. The Holocene 20 (2), 257–264. (69E)

Du, Naiqiu, Kong, Zhaochen, Shan, Fashou, 1989. A preliminary investigation on the vegetational and climatic changes since 11,000 years in Qinghai Lake. An analysis based on palynology in core QH85-14C. Acta Botanica Sinica 31, 803–814 (in Chinese).

Dykoski, C.A., Edwards, R.L., Cheng, H., Yuang, D.X., Cai, Y.J., Zhang, M.L., Lin, Y.S., Qing, J.M., An, Z.S., Revenaugh, J, 2005. A high-resolution absolute-dated Holocene and deglacial Asian monsoon record from Dongger Cave, China. Earth and Planetary Science Letters 233, 71–86.

Editorial Committee of Studies on Poyang Lake, 1987. Study on Poyang Lake. Shanghai Press of Science and Technology, Shanghai pp. 63 –69 (in Chinese). (65E)

Feng, S., Hu, Q., 2004. Variations in the Teleconnection of ENSO and Summer Rainfall in Northern China: A role of the Indian summer monsoon. Journal of Climate, 4871–4881.

Fleitmann, D., Burns, S.J., Mudelsee, M., Neff, U., Kramers, J., Mangini, A., Matter, A., 2003. Holocene forcing of the Indian monsoon recorded in a stalagmite from southern Oman. Science 300, 1737–1739.

Fleitmann, D, Burns, S.J., Mangini, A., Mudelsee, M., Kramers. J., Villa. I., Neff. U., Al-Subbary. A.A., Buettner, A, Hippler, D., Matter, A., 2007. Holocene ITCZ and Indian monsoon dynamics recorded in stalagmites from Oman and Yemen (Socotra). Quaternary Science Review 26, 170–188.

Gao, Shangyu, Chen, Weinan, Jin, Heling, Dong, Guangrong, Li, Baosheng, Yang, Gensheng, Liu, Lianyou, Guan, Youzhi, Sun, Zhong, Jin, Jiong, 1993. Preliminary study on the Holocene desert evolution on the northwestern margin of monsoon area in China. Science in China 23, 202–208. (31B)

Gasse, F., Arnold, M., Fontes, J.C., Fort, M., Gilbert, E., Huc, A., Li, Bingyan, Li, Yuanfang, Liu, Qing, Mélières, F., Van Campo, E., Wang, Fubao, Zhang, Qingsong, 1991. A 13,000-year climate record from western Tibet. Nature 353, 742 –745. (93H)

Geng, Kan, 1988. The geomorphologic features and evolution of the Holocene lakes in Dalainoer area, Inner Mongolia. Bulletin of Beijing Normal University (Natural Sciences) 4, 94–100 (in Chinese). (43B, 48B)

Goswami, B.N., Krishnamurthy, V., Annamalai, H., 1999. A broad-scale circulation index for the interannual variability of the Indian summer monsoon. Quarterly Journal of the Royal Meteorological Society 125, 611–633.

Gu, Zhaoyan, Liu, Jiaqi, Yuan, Baoyin, Liu, Tungsheng, Liu, Rongmo, Liu, Yu, Zhang, Guangyu, 1993. The evolution of the Qinghai-Xizang Plateau monsoon; evidence from the geochemistry of the sediments in Seling Co Lake. Chinese Science Bulletin 38, 61–64 (in Chinese). (92H)

Guo, Z.T., Berger, A., Yin, Q.Z.,Qin, L, 2009. Strong asymmetry of hemispheric climates during MIS-13 inferred from correlating China loess and Antarctica ice records. Climate of the Past 5, pp. 21–31. (26B)

Gupta, A.K., Das, M., Anderson, D.M., 2005. Solar influence on the Indian summer monsoon during the Holocene. Geophysical Research Letters 3, L17703, doi:10.1029/2005GL022685.

Han, Shuti, 1992. Holocene environmental change sequence of Barkol Lake, Northern Xinjiang. Scientia Geologica Sinica (Suppl.), 247–260 (in Chinese). (8A)

Haug, G.H., Hughen, K.A., Sigman, D.M., Peterson, L.C., Röhl, U., 2001. Southward migration of the Intertropical Convergence Zone through the Holocene. Science 293, 1304–1308.

He, Y., Theakstone, W., Zhang, Z., Zhang, D., Yao, T., Chen, T., Shen, Y., Pang, H., 2004. Asynchronous Holocene climatic change across China. Quaternary Research 61, 52–63.

Herzschuh, U., Tarasov, P., Wuennemann, B., Hartmann, K., 2004. Holocene vegetation and climate of the Alashan Plateau, NW China, reconstructed from pollen data. Palaeogeography, Palaeoclimatology, Palaeoecology 211, 1–17. (14B)

Herzschuh, U., 2006. Palaeo-moisture evolution in monsoonal central Asia during the last 50,000 years. Quaternary Science Reviews 25, 163–178. (91H)

Hewitt, C.D., Mitchell, J.F.B., 1998. A fully-coupled GCM simulation of the climate of the mid-Holocene. Geophysical Research Letters 25, 361–364.

Higginson, M.J., Altabet, A.A., 2004. A solar (irradiance) trigger for millennial-scale abrupt changes in the southwest monsoon? Paleoceanography 19, PA3015, doi:10.1029/2004PA001031.

Hong, Y.T, Hong, B., Lin, Q.H., Zhu, Y.X., Yasuyuki, S., Masashi, H., Masao, U., Leng, X.T., Jiang, H.B., Xu, H., H. Wang, H., Yi, L., 2003. Correlation between Indian Ocean summer monsoon and North Atlantic climate during the Holocene. Earth and Planetary Science Letters 211(3-4), 371–380. (22B)

Hong, Y.T, Hong, B., Lin, Q.H., Shibata Y., Hirota M, Zhu YX, Leng XT, Wang Y, Wang H, Yi L, 2005. Inverse phase oscillations between the east Asian and Indian Ocean summer monsoons during the last 12 000 years and paleo-El Nino. Earth and Planetary Science Letters 231, 337–346. (52C)

Hu, C., G.M. Henderson, J. Huang, S. Xie, Y. Sun, and K.R. Johnson, 2008: Quantification of Holocene Asian monsoon rainfall from spatially separated cave records. Earth and Planetary Science Letters 266, 221–232, doi:10.1016/j.epsl.2007.10.015. (71E)

Huang, Qi, Chai, Biqiang, Yu, Jungqing, 1980. The^{14}C dating and the Psedimentary cycle in the saline lakes on the Qinghai-Xizang Plateau. Chinese Science Bulletin 25, 990–994 (in Chinese). (9A)

Institute of Geochemistry, Chinese Academy of Sciences, 1977. Environmental changes in southern Liaoning Province during the last 10,000 years. Scientia Sinica, Series B 22, 603–614 (in Chinese). (58D)

Jarvis, D.I., 1993. Pollen evidence of changing Holocene monsoon climate in Sichuan Province, China. Quaternary Research 39, 325–337. (85G)

Ji, J., Shen, J., Balsam, W., Chen, J., Liu, L., Liu, X., 2005. Asian monsoon oscillations in the northeastern Qinghai-Tibet Plateau since the late glacial as interpreted from visible reflectance of Qinghai Lake sediments. Earth and Planetary Science Letters 233 (1-2), 61–70, doi:10.1016/j.epsl.2005.02.025.

Jiang, D., X. Lang, X., Tian, Z., Ju, L., 2013. Mid-Holocene East Asian summer monsoon strengthening: Insights from Paleoclimate Modeling Intercomparison Project (PMIP) simulations. Palaeogeography, Palaeoclimatology, Palaeoecology 369, 422–429.

Jiang, Q.H., Piperno, D.R., 1999. Environmental and archaeological implications of a late Quaternary palynological sequence, Poyang Lake, southern China. Quaternary Research 52, 250–258. (65E)

Jiang, W.Y., Gao, Z.T., Sun, X.J., Wu, H.B., Chu, G.Q., Yuan, B.Y., Hatté, C., Guiot, J., 2006. Reconstruction of climate and vegetation changes of the lake Bayanchagan (Inner Mongolia): Holocene variability of the East Asian monsoon. Quaternary Research 65, 411–420. (44B)

Jiang, W.Y., Leroy, S.A.G., Ogle, N., Chu, G.Q., Wang, L., Liu, J.Q., 2008. Natural and anthropogenic forest fires recorded in the Holocene pollen record from a Jinchuan peat bog, northeastern China. Palaeogeography, Palaeoclimatology, Palaeoecology 261, 47–57. (54C)

Jiang, Xiuyang, He, Yaoqi, Shen, Chuanzhou, Kong, Xinggong, Li, Zhizhong, Zhang, Yuwei, 2012. Stalagmite-inferred Holocene precipitation in northern Guizhou Province, China, and asynchronous termination of the Climatic Optimum in the Asian monsoon territory. Chinese Science Bulletin 57, 795–801, doi: 10.1007/s11434-011-4848-6. (73E)

Jin, L., Chen, F., Morrill, C., Otto-Bliesner, B.L., Rosenbloom, N., 2012. Causes of early Holocene desertification in arid central Asia. Climate Dynamics 38, 1577–1591, doi:

10.1007/s00382-011-1086-1.

Joussaume, S., Taylor, K. E., Braconnot, P., Mitchell, F. B., Kutzbach, E., Harrison, S. P., Prentice, I. C., Broccoli, A. J., Abe-Ouchi, A., Bartlein, P. J., Bonfils, C., Dong, B., Guiot, J., Herterich, K., Hewitt, C. D., Jolly, D., Kim, J. W., Kislov, A., Kitoh, A., Loutre, M. F., Masson, V., McAvaney, B., McFarlane, N., Noblet, N. D., Peltier, W. R., Peterschmitt, J. Y., Pollard, I. D., Rind, D., Royer, F., Schlesinger, M. E., Syktus, J., Thompson, S., Valdes, P., Vettoretti, G., Webb, R. S., and Wyputta, U., 1999. Monsoon changes for 6000 years ago: Results of 18 simulations from the Paleoclimate Modeling Intercomparison Project (PMIP). Geophysical Research Letters 26, 859–862.

Kelts, K., Zao, C.K., Lister, G., Hong, G.Z., Niessen, F., Bonani, G., 1989. Geological fingerprints of climatic history; a cooperative study of Qinghai Lake, China. Ecologae Geology 82, 167 –182. (12B)

Khon, V. C., Park, W., Latif. M., Mokhov, I.I., Schneider, B., 2010. Response of the hydrological cycle to orbital and greenhouse gas forcing. Geophysical Research Letters 37, L19705, doi:10.1029/2010GL044377.

Koutavas, A., deMenocal, P.B., Olive, G.C., Lynch-Stieglitz, J., 2006. Mid-Holocene El Niño-Southern Oscillation (ENSO) attenuation revealed by individual foraminifera in eastern tropical Pacific sediments. Geology 34, 993–996.

Kutzbach, J.E., 1981. Monsoon climate of the early Holocene: climate experiment using the earth’s orbital parameters for 9000 years ago. Science 214, 59–61.

Kutzbach, J.E., Otto-Bliesner, B.L., 1982. The sensitivity of the African-Asian monsoonal climate to orbital parameter changes for 9000 years B.P. in a low-resolution general circulation model. Journal of Atmospheric Science 39, 1177–1188.

Latif, M., Park, W., Ding, H., Keenlyside, N. S., 2009. Internal and external North Atlantic Sector variability in the Kiel Climate Model. In: Meteorologische Zeitschrift 18 (2009), Nr. 4, S. 433–443.

Lau, N., Nath, M., 2006. ENSO modulation of the interannual and intraseasonal variability of the East Asian monsoonda model study. Journal of Climate 19, 4508–4530.

Levitus, S., 1982. Climatological Atlas of the World Ocean, NOAA/ERL GFDL Professional Paper 13, Princeton, N.J., 173 pp. (NTISPB83-184093).

Li, Huazhang, Liu, Qingsi, Wang, Jiaxing, 1992a. Study of evolution of Huangqihai and Daihai Lakes in Holocene in Inner Mongolia Plateau. Journal of Lake Sciences 4 (1), 31–39 (in Chinese). (40B)

Li, Pingri, Zheng, Jiansheng, Fang, Guoxiang, 1991. Quaternary Geology in the Guangzhou area. Printing House of the Huanan University of Science and Technology, pp. 53-81 (in Chinese). (76F, 77F)

Li, Wenyi, Liang, Yulian, 1985. Vegetation and environment of the hypsithermal interval of Holocene in the eastern Hebei Plain. Acta Botanica Sinca 27, 640–651 (in Chinese). (56D)

Li, Wenyi, Liu, Guangxiu, Zhou, Mingming, 1992b. The vegetation and climate of the Holocene Hypsithermal in Northern Hubei Province. In: Shi, Y.F. (Ed.), The Climate and environments of Holocene Megathermal in China. China Ocean Press, Beijing: pp. 94–99 (in Chinese). (68E, 70E)

Li, Wenyi, Liu, Guangxiu, Liang, Yulian, Xu, Qinghai, 1993. Forest history and environmental changes in Bajiaotian of Miaoershan Mt. In: Li, W.Y., Yao, Z.J. (Eds.), Late Quaternary Vegetation and Environment of North and Middle Subtropical Region of China. Ocean Press, Beijing, China, pp. 121–132 (in Chinese). (72E)

Li, Xiaoqiang, An, Zhisheng, Zhou, Jie, Gao, Huijun, Zhao, Hongli, 2003. Characteristics of vegetation in the Loess Plateau area since Holocene. Marine Geology & Quaternary Geology 23, 109–114 (in Chinese). (28B, 29B)

Li, X.Q., Zhou, W.J., An, Z.S., Dodson, J., 2003. The vegetation and monsoon variations at the desert-loess transition belt at Midiwan in northern China for the last 13 ka. The Holocene 13, 779–784. (28B, 29B)

Li, Y. and Morrill, C., 2010. Multiple factors causing Holocene lake level change in monsoonal and arid central Asia as identified by model experiments. Climate Dynamics 35,1119–1132.

Lin, Shaomeng, 1987. The vegetation history from the late Pleistocene to Holocene at Eryuan, Yunnan Province. In: Sino-Australia Cooperative Group (Ed.). Contributions to the Quaternary Symposium. Science Press, Beijing, pp. 56 –67 (in Chinese). (86G, 87G)

Lin, Shuji, Zheng, Honghan, 1987. Evolution of Caohai Lake. Guizhou People's Press, Guiyang: pp. 7–38 (in Chinese). (81G)

Liu, G.X., Li, W.Y., Chou, M.M., 1993. Study of modern pollen rain at Dajiuhu area. In: Li, W.Y., Yao, Z.J. (Eds.), Late Quaternary Vegetation and Environment of North and Middle Subtropical Region of China. Ocean Press, Beijing, China, pp. 121–132 (in Chinese). (68E)

Liu, H., Xu, L., Cui, H., 2002. Holocene history of desertification along the woodland–steppe border in northern China. Quaternary Research 57, 259–270. (46B, 47B)

Liu, J., 1989. Vegetational and climatic changes at Gushantun Bog in Jilin, NE China since 13,000 a BP. Acta Palaeontologica Sinica 28, 240–248 (in Chinese). (51C, 53C)

Liu, K.-B, Qiu, H., 1994. Late Holocene pollen records of vegetational changes in China: climate or human disturbance. Tao 5, 393–410. (12B)

Liu, K.-B, S, S., Jiang, X., 1992. Environmental change in the Yangtze River Delta since 12,000 years B.P. Quaternary Research 38, 32–45. (61E)

Liu, K.-B., Yao, Z.J., Thompson, L.G., 1998. A pollen record of Holocene climatic changes from Dunde ice cap, Qinghai–Tibetan Plateau. Geology 26, 135–138. (10A)

Liu, Z., Harrison, S.P., Kutzbach, J., Otto-Bliesner, B., 2004. Global monsoons in the mid-Holocene and oceanic feedback. Climate Dynamics 22, 157-182, doi:10.1007/s00382-003-0272-y.

Liu, Z., Kutzbach, J., Wu, L., 2000. Modeling climate shift of El Nino variability in the Holocene. Geophysical Research Letters 27(15), 2265–2268, doi: 10.1029/2000GL011452.

Lorenz, S., Lohmann, G., 2004. Acceleration technique for Milankovitch type forcing in a coupled atmosphere-ocean circulation model: method and application for the Holocene. Climate Dynamics 23, 727–743, doi:10.1007/s00382-004-0469-y.

Madec, 2008. NEMO reference manual, ocean dynamics component: NEMO-OPA. Preliminary version. Note Pole Model. 27, Inst. Pierre Simon Laplace, Paris.

Maher, B.A., 2008. Holocene variability of the east Asian summer monsoon from Chinese cave records: a re-assessment. The Holocene 18, 861–866.

Maher, B.A., Hu, M., 2006. A high-resolution record of Holocene rainfall variations from the western Chinese Loess Plateau: antiphase behaviour of the African/Indian and east Asian summer monsoons. The Holocene 16, 309–319.

Mayewski, P.A., Rohling, E.E., Stager, C.J., Karlén, W., Maasch, K.A., Meeker, L.D., Meyerson, E.A., Gasse, F., Van Kreveld, S., Holmgren, K., Lee-Thorp, J., Rosqvist, G., Rack, F., Staubwasser, M., Schneider, R.R., Steig, E.J., 2004. Holocene climate variability. Quaternary Research 62, 243–255.

Mitchell, J.F.B, Grahame, N.S., Needam, K.J., 1988. Climate simulation for 9000 years before present: Seasonal variations and effect of the Laurentide Ice Sheet. Journal of Geophysical Research 93 (D7), 8283–8303.

Mitchell, T.D., Jones, P.D., 2005. An improved method of constructing a database of monthly climate observations and associated high-resolution grids. International Journal of Climate 25, 693–712.

Morrill, C., Overpeck, J.T., Cole, J.E., Liu, K.-B., Shen, C., Tang, L., 2006. Holocene variations in theAsian monsoon inferred from the geochemistry of lake sediments in central Tibet. Quaternary Research 65, 232–243.

Moy, C.M., Seltzer, G.O., Rodbell, D.T., Anderson, D.M., 2002. Variability of El Niño-Southern

Oscillation activity at millennial time scales during the Holocene epoch. Nature 420, 162–165.

Nanjing Institute of Geography, and Limnology (CAS), 1989. Environments and Sedimentation of Fault Lake, Yunnan Province. Science Press, Beijing (in Chinese). (84G)

Otto-Bliesner, B. L., Brady, E.C., Shin, S.I., Z. Liu, Z., Shields, C., 2003. Modeling El Niño and its tropical teleconnections during the last glacial-interglacial cycle. Geophysical Research Letters 30(23), 2198, doi:10.1029/2003GL018553.

Overpeck, J., Anderson, D., Trumbore, S., Prell, W., 1996. The southwest Indian monsoon ove the last 18,000 years. Climate Dynamics 12, 213–225.

Park, W., Latif, M., 2008. Multidecadal and multicentennial variability of the meridional overturning circulation. Geophysical Research Letters 35, L22703. doi:10.1029/2008GL035779.

Park, W., Keenlyside, N., Latif, M., Stroeh, A., Redler, R., Roeckner, E. and Madec, G., 2009. Trpocal Pacific climate and its response to global warming in the Kiel Climate Miodel. Journal of Climate 22, 71–92.

Park, W., Latif, M., 2010. Pacific and Atlantic multidecadal variability in the Kiel Climate Model. Geophysical Research Letters 37, L24702. doi:10.1029/2010GL045560.

Parthasarathy, B., Munot, A.A., Kothawale, D.R., 1994. All-India Monthly and Seasonal Rainfall Series: 1871-1993. Theoretical and Applied Climatology 49, 217–224.

Rodbell, D.T., Seltzer, G.O., Anderson, D.M., Abbott, M.B., Enfield, D.B., Newman, J.H., 1999. An ~15,000-year record of El Niño–Driven Alluviation in southwestern Ecuador. Science 283, 516-520.

Roeckner, E., Bäuml, G., Bonaventura, L., Brokopf, R., Esch, M., Giorgetta, M., Hagemann, S., Kirchner, I., Kornblueh, L., Manzini, E., Rhodin, A., Schlese, U., Schulzweida, U., Tompkins, A., 2003. The atmospheric general circulation model ECHAM5. Part I: Model description, Rep. 349, 127pp., ISSN 0937-1060, Max Planck Institut für Meteorologie, Hamburg, Germany.

Ruddiman, W.F., 2008. Earth’s Climate: Past and Future, second ed. W.H. Freeman and Company, New York, pp.138–142.

Selvaraj, K., Chen, C.T.A., Lou, J.-Y., 2007. Holocene East Asian monsoon variability: Links to solar and tropical Pacific forcing. Geophysical Research Letters 34, L01703, doi:10.1029/2006GL028155.

Shen, C.M., 2003. Millennial-scale variations and centennial-scale events in the Southwest Asian monsoon: pollen evidence from Tibet. PhD Dissertation, Louisiana State University, Banta Rouge. (90H)

Shen, J., Liu, X.Q.,Wang, S.M., Matsumoto, R., 2005. Palaeoclimatic changes in the Qinghai Lake area during the last 18,000 years. Quaternary International 136, 131–140. (12B)

Shen, J., Jones, R.T., Yang, X.D., Dearing, J.A., Wang, S.M., 2006. The Holocene vegetation history of Lake Erhai, Yunnan province southwestern China: the role of climate and human forcings. The Holocene 16, 265–276. (87G)

Shi, Peijun, Song, Changqing, 2003. Palynological records of environmental changes in the middle part of Inner Mongolia, China. Chinese Science Bulletin 48, 1433–1438. (37B)

Shi, Yafeng, 1990. Quaternary Climatic Environmental Change and Hydrogeologic Events in Caiwopo Basin in Xinjiang. Ocean Press, Beijing, pp. 46–72 (in Chinese). (6A)

Shi, Z., Liu, X., Cheng, X., 2012. Anti-phased response of northern and southern East Asian summer precipitation to ENSO modulation of orbital forcing. Quaternary Science Reviews 40, 30–38.

Shukla, J., Paolino, D.A., 1983. The southern oscillation and long-range forecasting of the summer monsoon rainfall over India. Monthly Weather Review 111, 1830–1837.

Song, Xieliang, 1994. Palaeolimnological Studies on the Limestone District in Central Yunnan. Science and Technology Press, Beijing (in Chinese). (83G)

Staubwasser, M., Sirocko, F., Grootes, P.M., Segl, M., 2003. Climate change at the 4.2 ka BP termination of the Indus valley civilization and Holocene south Asian monsoon variability. Geophysical Research Letters 30, 1425, doi: 10.1029/2002GL016822.

Sun, Dapeng, 1990. The soda Lakes on the Inner Mongolia Plateau, China. Oceanologia et Limnologia Sinica 21, 44–53 (in Chinese). (41B)

Sun, Jianzhong, Zhao, Jinbo, 1991. Quaternary of the Loess Plateau. Science Press, Beijing pp 186–205 (in Chinese). (33B)

Sun, Shuncai, Wu, Yifan, 1987a. The formation and evolution of Taihu Lake and sedimentation. Science in China (B) 30, 1329–1339 (in Chinese). (62E)

Sun, Xiangjun, Du, Naiqin, Chen, Yinshuo, Gu, Zhaoyan, Liu, Jiaqi, Yuan, Baoyin, 1993. Holocene palynological records in Lake Selinco, Northern Xizang. Acta Botanica Sinica 35, 943–950 (in Chinese). (92H)

Sun, Xiangjun, Du, Naiqin, Weng, Chengyu, Lin, Ruifeng, Wei, Keqin, 1994. Paleovegetation and paleoenvironment of Manas Lake, Xinjiang, N.W. China during the last 14,000 years. Quaternary Sciences 3, 239–246 (in Chinese with English Abstract). (4A)

Sun, Xiangjun, Wu, Yushu, 1987b. Holocene vegetation history and environmental changes of the Dianchi Lake area, Yunnan Province. Proceedings of China-Australia Academia Symposium on Quaternary Geology. Science Press, Beijing, pp. 28–41 (in Chinese) (82G)

Sun, Xiangjun, Yuan, Shaomin, 1990. Pollen data and evolution of the vegetation for the last 10,000 years in Jinchuan basin, Jiling Province. In: Loess, Quaternary Geology, and Global Change, Vol. 2. Science Press, Beijing, pp. 46–47 (in Chinese). (54C)

Tan, Qixiang, 1980. Yunmen and Yunmence. Bulletin of Futan Univer-sity (Special Issue on Historical Geography) 1911 (in Chinese). (67E)

Tang, Lingyu, Shen, Caiming, 1992. The vegetation and climates of the Holocene Megathermal in northern Jiangsu Province. In: Shi, Y.F. (Ed.), The climates and environments of the Holocene Megathermal in China. Chinese Ocean Press, Beijing pp. 80–93 (in Chinese). (60E)

Tang, Lingyu, Shen, Caiming, Liu, K.-B., Overpeck, J.T., 2000. Changes in south Asian monsoon: new high-resolution paleoclimatic records from Tibet, China. Chinese Science Bulletin 45, 87–91. (89H)

Tarasov, P., Jin, G.Y., Wagner, M., 2006. Mid-Holocene environmental and human dynamics in northwestern China reconstructed from pollen and archaeological data. Palaeogeography, Palaeoclimatology, Palaeoecology 241, 284–300. (45B)

Tiwari, M., Ramesh, R., Somayajulu, B.L.K., Jull, A.J.T., Burr, G.S., 2005. Solar control of southwest monsoon on centennial timescales. Current Science 89, 1583–1589.

Tiwari, M., Ramesh, R., Bhushan, R., Sheshshayee, M.S., Somayajulu, B.L.K., Jull, A.J.T., Burr, G.S., 2010. Did the Indo-Asian summer monsoon decreasing during the Holocene following insolation? Journal of Quaternary Science 25, 1179–1188, ISSN 0267–8179.

Valcke, S., 2006. OASIS3 user guide, PRISM Tech. Rep. 3, 64 pp., Partnership for Res. Infrastructures in Earth Syst. Model., Toulouse, France. (Available at http://www.prism.enes.org/Publications/Reports/oasis3_UserGuide_T3.pdf)

Van Campo, E., Gasse, F., 1993. Pollen- and diatom-inferred climatic and hydrological changes in Sumxi Co Basin (Western Tibet) since 13,000 yr B.P. Quaternary Research 39, 300–313. (1A)

Van Campo, E., Cour, P., Hang, S.X., 1996. Holocene environmental changes in Bangong Co basin (Western Tibet). Part 2: the pollen record. Palaeogeography, Palaeoclimatology, Palaeoecology 120, 49–63. (94H)

Wang, B., Lin, H., 2002. Rainy season of the Asian-Pacific summer monsoon. Journal of Climate 15, 386-396.

Wang, B., Wu, R., Fu, X., 2000. Pacific-East Asian teleconnection: how does ENSO affect East Asian climate? Journal of Climate 13, 1517–1536.

Wang, B., Wu, R., Li, T., 2003. Atmosphere-warm ocean interaction and its impacts on AsianeAustralian monsoon variation. Journal of Climate 16, 1195–-1211.

Wang, B., Wu, Z., Li, J., Liu, J., Chang, C-P, Ding, Y., Wu, G., 2008. How to measure the strength of the East Asian summer monsoon. Journal of Climate 21, 4449–4463.

Wang, Bengyu, Sun, Xiangjun, 1997. Preliminary study of Holocene environmental change in Chasuqi. Chinese Science Bulletin 42, 514–518 (in Chinese). (36B)

Wang, Shilan, Chen, Fahu, Cao, Jixiu, 1991. The pollen assemblage and climatic fluctuations in Lanzhou River Basin since 10,000 a B.P. Journal of Glaciology and Geocryology 13, 307–314 (in Chinese). (19B)

Wang, Sumin, Ji, Lei, Yang, Xiangdong, Xue, Bin, Ma, Yan, Hu, Shouyun, 1994. Record of Younger Dryas event in the lacustrine in Zhalainuoer of Inner Mongolia. Chinese Science Bulletin 39, 348–351 (in Chinese). (50C)

Wang, Sumin, Wu, Ruijin, Jiang, Xinhe, 1990a. Environmental evolution and paleoclimate of Daihai Lake, Inner Mongolia, since the last glaciation. Quaternary Sciences 3, 223–232 (in Chinese). (38B)

Wang, Sumin, Yu, Yuansheng, Wu, Ruijin, Feng, Min, 1990b. Daihai Lake environmental evolution and climate change. Printing House of University of Science and Technology of China, pp. 117–182 (in Chinese). (38B)

Wang, Shuyun, Lu, Houyuan, Liu, Jiaqi, Negendank, J.F.W., 2007. Early Holocene climate optimum revealed by high-resolution pollen record from Huguangyan Maar Lake. Chinese Science Bulletin 52, 1285–1291. (78F)

Wang, Y.J., Cheng, H., Edwards, R.L., He, Y.Q., Kong, X.G., An, Z.S., Wu, J.Y., Kelly, M.J., Dykoski, C.A., Li, X.D., 2005. The Holocene Asian monsoon links to solar changes and North Atlantic climate.

Science 308, 854–857. (74E)

Wang, Y., Liu, X, Herzschuh, U., 2010. Asynchronous evolution of the Indian and east Asian summer monsoon indicated by Holocene moisture patterns in monsoonal central Asia. Earth-Science Reviews 103, 135–153.

Webster, P. J.,Yang, S., 1992. Monsoon and ENSO: Slectively interactive systems. Quarterly Journal of the Royal Meoterological Society 118, 877–926.

Weber, S.L., Crowley, T.J., van der Schrier, G., 2004. Solar irradiance forcing of centennial climate variability during the Holocene. Quaternary Science Reviews 22, 539–553.

Wu, Jinglu, Wang, Sumin, Wang, Hongdao, 1996. Characters of the evolution of climate and environment of Holocene in Aibi Lake Basin in Xinjiang. Oceanologia et Limnologia Sinica 27, 524–530 (in Chinese). (3A)

Xia, Yumei, 1988. A preliminary study on vegetational development and climatic changes in the Sanjiang Plain since 12,000 yr B.P. Scientia Geographica Sinica 8, 240–249 (in Chinese). (55C)

Xiao, J.L., Xu, Q.H., Nakamura, T., Yang, X.L., Liang, W.D., Inouchi, Y., 2004. Holocene vegetation variation in the Daihai Lake region of north-central China: a direct indication of the Asian monsoon climatic history. Quaternary Science Reviews 23, 1669–1679. (38B)

Xiao, Jiayi, Lu, Haibo, Zhou, Weijian, Zhao, Zhijun, Hao, Ruihui, 2007. Evolution of vegetation and climate since the last glacial maximum recorded at Dahu peat site, south China. Science in China (Series D) 50, 1209–1217. (75F)

Xu, Qinghai, Chen, Shuying, Kong, Zhaochen, Du, Naiqiu, 1988. Preliminary discussion of vegetation succession and climate change since the Holocene in the Baiyangdian Lake district. Acta Phytoecologica et Geobotanica Sinica 12, 143–151 (in Chinese). (57D)

Xu, Xin, Zhu, Minglun, 1984. The vegetational and climatic changes in the Zhenjiang region since

15,000 years B.P.. Acta Geographica Sinica 39, 277–284. (63E)

Xu, Yingqin, 1998. The assemblage of Holocene spore pollen and its environment in Boston Lake area Xinjiang. Arid Land Geography 21 (2), 43–49 (in Chinese). (7A)

Yan, G., Wang, F.B., Shi, G.R., Li, S.F., 1999. Palynological and stable isotopic study of palaeoenvironmental changes on the northeastern Tibetan Plateau in the last 30,000 years. Palaeogeography, Palaeoclimatology, Palaeoecology 153, 147–159. (80G)

Yang, X., Scuderi, L., 2010. Hydrological and climatic changes in deserts of China since the late Pleistocene. Quaternary Research 73, 1–9. (15B)

Yang, X., Scuderi, L., Paillou, P., Liu, Z., Ren, X., 2011. Quaternary environmental changes in the drylands of China - A critical review. Quaternary Science Reviews 30, 3219-3233. (2A)

Yang, Xiangdong, Wang, Sumin, 1996. The vegetation and climatic environmental changes in Hunlun Lake and Wulun Lake during Holocene. Oceanologia et Limnologia Sinica 27, 67–72 (in Chinese). (5A, 49C)

Yang, X, Zhu, B., Wang, X., Li, C., Zhou, Z., Chen, J., Wang, X., Yin, J., Lu, Y., 2008. Late Quaternary environmental changes and organic carbon density in the Hunshandake Sandy Land, eastern Inner Mongolia, China. Global and Planetary Change 61, 70–78. (42B)

Yeh, Tucheng, Dao, Shihyen, Li, Meitsiun, 1958. The abrupt change of circulation over Northern Hemisphere during June and October. Acta Meteorologica Sinica 29 (4), 249–263 (in Chinese).

Yi, S., Saito, Y., Oshima, H., Zhou, Y.Q., Wei, H.L., 2003. Holocene environmental history inferred from pollen assemblages in the Huanghe (Yellow River) delta, China: climatic change and human impact. Quaternary Science Reviews 23, 609–628. (59D)

Yuan, Baoyin, 1988. Geological significance of the climatic geomorphology of the Late Pleistocene in North China. Acta Scientiarum Naturalism Universitatis Pekinensis 24, 235–244 (in Chinese). (30B)

Zhang, H.C., Ma, Y.Z., Wuennemann, B., Pachur, H.-J., 2000. A Holocene climatic record from arid northwestern China. Palaeogeo- graphy, Palaeoclimatology, Palaeoecology 162, 395–397. (17B)

Zhang, J.W., Chen, F.H., Holmes, J.A., Li, H., Guo, X.Y., Wang, J.L., Li, S., Lü, Y.B., Zhao, Y., Qiang, M.R., 2011. Holocene monsoon climate documented by oxygen and carbon isotopes from lake sediments and peat bogs in China: a review and synthesis. Quaternary Science Reviews 30, 1973–1987.

Zhang, Xiaoyang, 1991. The formation and evolution of Dongting Lake and delta deposit. M.S. Thesis, Nanjing Institute of Geography (in Chinese). (66E)

Zhao, Y., Yu, Z.C., Chen, F.H., Ito, E., Zhao, C., 2007. Holocene vegetation and climate history at Hurleg Lake in the Qaidam Basin, northwest China. Review of Palaeobotany and Palynology 145, 275–288. (11A)

Zhao, Y., Chen, F.H., Zhou, A.F., Yu, Z.C., 2010. Vegetation history, climate change and human activities over the last 6200 years on theLiupan Mountains in the southwestern Loess Plateau in central China. Palaeogeography, Palaeoclimatology, Palaeoecology 293, 197–205. (25B)

Zhao, Y.,Yu, Z.C,, Chen, F.H., 2009a. Spatial and temporal patterns of Holocene vegetation and climate changes in arid and semi-arid China. Quaternary International 194, 6–18

Zhao, Y., Yu, Z.C., Chen, F.H., Zhang, J.W., Yang, B., 2009b. Vegetation response to Holocene climate change in monsoon-influenced region of China. Earth-Science Reviews 97, 242–256.

Zhao. Y., Yu, Z.C., Zhao, W.W., 2011. Holocene vegetation and climate histories in the eastern Tibetan Plateau: controls by insolation-driven temperature or monsoon-derived precipitation changes? Quaternary Science Reviews 30, 1173–1184. (21B)

Zhao, Y., Yu, Z.C., 2012. Vegetation response to Holocene climate change in East Asian mon- soon-margin region. Earth-Science Reviews 113, 1–10.

Zheng, Zhuo, Wang, Jianghua, Wang, Bing, Liu, Chunlian, Zou, Heping, Zhang, Hua, Deng, Yun, Bai, Yan, 2003. High-resolution records of Holocene from Shuangchi Maar Lake in Hainan Island. Chinese Science Bulletin 48 (50, 497–502. (79F)

Zhou, Mingfu, Shen, Chengde, Huang, Baolin, Qiao, Yulou, 1992. 14C chronology of the variation of Fuxian Lake and the neotectonic movement of Chengjiang basin in Yunnan Province during the last 50 ka. In: Loess, Quaternary Geology, and Global Change, 3. Science Press, Beijing, pp. 155–160 (in Chinese). (81G)

Zhou, Weijian, An, Zhisheng, 1991. 14C chronology of Loess Plateau in China. In: Liu, Tungsheng (Ed.), Quaternary Geology and Environ-ment in China. Science Press, Beijing, pp. 192–200 (in Chinese). (32B, 34B)

Zhou, W.J., Yu, X.F., Timothy J., A.J., Burr, G., Xiao, J.Y., Lu, X.F., Xian, F., 2004. High resolution evidence from southern China of an early Holocene optimum and a mid-Holocene dry event during the past 18,000 years. Quaternary Research 62, 39–48. (75F)

Zhu, Cheng, Ma, Chunmei, Zhang, Wenqing, Zheng, Chaogui, Tang, Lingyu, Lu, Xuefeng, Liu, Kexin, Chen, Huizhong, 2006. Pollen record from Dajiuhu Basin of Shennongjia and environmental changes since 15.753 kaB.P. Quaternary Sciences 5, 814–826 (in Chinese with English abstract). (70E)

Zhu, Haihong, 1989. Lacustrine Environment and Sediments of the Yunnan Fault-Downwarped Lakes. Science Press, Beijing (in Chinese). (82G)

Table 1

Boundary conditions used in KCM simulations.

	Eccentricity	Obliquity (º)	Precession (ω−180º)	CO_2 (ppm)	CH_4 (ppb)	N_2O (ppb)
H0K	0.0167	23.4	102	286.2	805.6	276.7
H9K	0.0194	24.2	303	same as H0K		
HT	varying from H9K to H0K			same as H0K		

Table 2

List of proxy record sites from different regions in this study (Each of the references is noted in the References of the text with site NO.)

Site NO.	Site name	Latitude(N)	Longitude(E)	Reference
1A	Sumxi Co(N)	35°30′	81°00′	Van Campo and Gasse (1993)
2A	Taklamakan	37°-42°	75°-90°	Yang et al. (2011)
3A	Aibi Lake	44°54′	82°35′	Wu et al. (1996)
4A	Manas Lake	45°45′	86°00′	Sun et al. (1994)
5A	Wulun Lake	46°59′	87°00′	Yang and Wang (1996)
6A	Chaiwopo	43°25′	87°15′	Shi (1990)
7A	Boston Lake	41°56′	86°40′	Xu (1998)
8A	Balikun	43°42′	92°44′	Han (1992)
9A	Daqaidan	37°50′	95°15′	Huang et al. (1980)
10A	Dunde	38°06′	96°24′	Liu et al. (1998)
11A	Hurleg Lake	37°19′	96°54′	Zhao et al. (2007)
12B	Qinghai lake	36°32′	99°36′	Du et al. (1989) Kelts et al. (1989) Liu and Qiu (1994) Shen et al. (2005)
13B	Halali	36°40′	99°53′	Chen et al. (1991a)
14B	Eastern Juyanze	41.89°	101.85°	Herzschuh et al. (2004)
15B	Badain Jaran	38°-43°	99°-107°	Yang et al. (2010)
16B	Sanjiaocheng	39°00′	103°20′	Chen et al. (2006)
17B	Hongshui River	38°10′46″	102°45′53″	Zhang et al. (2000)
18B	Jiuzhoutai	36°05′	103°48′	Chen et al. (1991b)
19B	Lanzhou	36°03′	103°73′	Wang et al. (1991)
20B	Baxie	35°34′	103°35′	An et al. (1993)
21B	Zoige peatland	33.5°	103°	Zhao et al. (2011)
22B	Hongyuan	32°46′	102°31′	Hong et al. (2003)
23B	Sujiawan	35°32′20″	104°31′22″	An et al. (2003)
24B	Dadiwan	35°01′	105°54′	An et al. (2003)
25B	Tianchi Lake	35°16′	106°19′	Zhao (2010)
26B	Xifeng	35°42′	107°38′	Guo et al. (2009)
27B	Jiuxian	33°34′	109°06′	Cai et al. (2010)
28B	Yaoxian	34°56′	108°50′	Li et al. (2003)
29B	Midiwan	37°39′	108°37′	Li et al. (2003)
30B	Salawusu	37°50′	108°40′	Yuan (1988)
31B	Sandaogou	38.4°	109.25°	Gao et al. (1993)
32B	Luochuan	35°44′	109°25′	Zhou and An (1991)
33B	Fuping	34°50′	109°50′	Sun and Zhao (1991)
34B	Beizhuangcun	34°22′	109°32′	Zhou and An (1991)
35B	Wudangzhao	40°50′	110°15′	Cui and Song (1992)
36B	Chasuqi	40°40′	111°08′	Wang and Sun (1997)
37B	Diaojiao Lake	41°18′	112°21′	Shi and Song (2003)
38B	Daihai Lake	40°35′	112°40′	Wang et al. (1990a,b) Xiao et al. (2004)
39B	Baisuhai	41°08′	112°40′	Cui and Song (1992)
40B	Huangqihai	40°50′	113°15′	Li et al. (1992a)
41B	Chaganlimenoer	43°16′	112°53′	Sun (1990)
42B	Hunshandake	42°-44°	112°-118°	Yang et al. (2008)
43B	Chanhanzhao	41°30′	113°52′	Geng (1988)
44B	Bayanchagan	41.65°	115.21°	Jiang et al. (2006)
45B	Taishizhuang	40°21.5′	115°49.5′	Tarasov et al. (2006)
46B	Xiaoniuchang	42°37′	116°48′	Liu et al. (2002)
47B	Haoluku	42°57.38′	116°45.42′	Liu et al. (2002)
48B	Dalainoer	43°20′	116°40′	Geng (1988)

49C	Hulun Lake	48°30′40″	116°58′	Yang and Wang (1996)
50C	Hulong Lake	49°00′	117°20′	Wang et al. (1994)
51C	Gushantong	42°30′	126°10′	Liu (1989)
52C	Hani	42.21°	126.21°	Hong et al. (2005)
53C	Gushantun	42°30′	126°10′	Liu (1989)
54C	Jinchuan	42°20′	126°22′	Sun and Yuan (1990) Jiang et al. (2008)
55C	Qindeli	48°00′	133°15′	Xia (1988)
56D	Maohebei	39°32′	119°12′	Li and Liang (1985)
57D	Baiyangdian	38°50′	116°00′	Xu et al. (1988)
58D	Pulandian	39°30′	112°00′	Institute of Geochemistry (1977)
59D	Yellow River Delta	37°47.8′2	118°54.3′	Yi et al. (2003)
60E	Jianhu	33°30′	119°45′	Tang and Shen (1992)
61E	Qidong	31°50′	121°40′	Liu et al. (1992)
62E	Taihu Lake	30°55′-31°35′	119°50′-120°35′	Sun and Wu (1987a)
63E	Zhenjiang	32°12′	119°25′	Xu and Zhu (1984)
64E	Chao Lake	31°25′28″	117°16′54″	Chen et al. (2009)
65E	Poyang Lake	28°52′	116°15′	Editorial Committee of a Studies on Poyang Lake (1987) Jiang and Piperno (1999)
66E	Dongting Lake	28°40′-29°30′	111°45′-113°10′	Zhang (1991)
67E	Guyuanmence	29°40′-30°20′	111°40′-112°25′	Tan (1980)
68E	Longquan Lake	30°53′	111°52′	Li et al. (1992b) Liu et al. (1993)
69E	Sanbao	31°40′	110°26′	Dong et al. (2010)
70E	Dajiuhu Lake	31°25′	110°10′	Li et al. (1992b) Zhu et al. (2006)
71E	Heshang	30°27′	110°25′	Hu et al. (2008)
72E	Bajiaotian	25°48′	110°20′	Li et al. (1993)
73E	Shigao	28°11′	107°10′	Jiang et al. (2012)
74E	Dongge	25°17′	108°05′	Wang et al. (2005)
75F	Dahu	24°41′	115°	Zhou et al. (2004) Xiao et al. (2007)
76F	Fangyu	22°55′	113°25′	Li et al. (1991)
77F	Huangsha	23°10′	110°20′	Li et al. (1991)
78F	Huguang Maar Lake	21°9′	110°17′	Wang et al. (2007)
79F	Shuangchi Maar Lake	19°57′	110°11 ′	Zheng et al. (2003)
80G	Zoige Basin	32°20′	103°25′	Yan et al. (1999)
81G	Caohai Lake	26°50′	104°12′	Lin and Zheng (1987) Zhou et al. (1992)
82G	Dianchi	24°40′-25°03′	102°35′-40′	Sun et al. (1987b) Zhu (1989)
83G	Fuxian Lake	24°25′-35′	102°50′-55′	Song (1994)
84G	Jimenghai	24°10′	102°45′	Nanjing Institute of Geography and Limnology, CAS (1989)
85G	Shayema Lake	28°05′	101°35′	Jarvis (1993)
86G	Eryuan	26°08′	99°55′	Lin (1987)
87G	Erhai Lake	25°36′	100°05′	Lin (1987) Shen et al. (2006)
88H	Mawmluh	25°16′	91°53′	Berkelhammer et al. (2012)
89H	Hidden Lake	29°49′	92°48′	Tang et al. (2000)
90H	Qongjiamong Co	29°48.77′	92°22.37′	Shen (2003)
91H	Zigetang Lake	32.0°	90.9°	Herzschuh et al. (2006)
92H	Seling Co	31°34′-37′	88°31′-89°21′	Gu et al. (1993) Sun et al. (1993)
93H	Sumxi Co(S)	34°18′	80°08′	Gasse et al. (1991)
94H	Bangong Lake	33°40′	79°00′	Van Campo et al. (1996)

4

Figure captions

Fig. 1. Comparison of annual mean precipitation (mm/day) (a, c) and annual mean surface temperature (ºC) (b, d) from the Climate Research Unit TS 2.1 dataset for 1901-1930 (a, b) and KCM pre-industrial simulation (c, d).

Fig. 2. Insolation changes (W/m^2) in boreal summer (June) (solid lines) and winter (December) (dash lines) (Berger and Loutre, 1991), shown as deviations relative to 9.5 ka BP. The 9.5 ka BP insolation at 30ºN is 509.87 (W/m^2) for June and 207.07 (W/m^2) for December, respectively.

Fig. 3. Simulated boreal summer (June-July-August, JJA) surface temperature (ºC) over Eurasian continent at 0 ka BP relative to 9.5 ka BP.

Fig. 4. Asian summer monsoon indices calculated from HT simulation with a 99-point smoothing average. Black line indicates the Indian summer monsoon index (*ISMI*), and the red line indicates the East Asian summer monsoon index (*EASMI*). Both the *ISMI* and *EASMI* values are relative to values of 9.5 ka BP, respectively. The *ISMI* is adapted from Goswami et al. (1999) as the difference of JJA meridional wind anomalies at 850 hPa and 200 hPa averaged over the ISM region (70ºE-110ºE, 10ºN-30ºN), i.e. $ISMI = V^*_{850} - V^*_{200}$, where V^*_{850} and V^*_{200} are boreal summer season (JJA) meridional wind anomalies at 850 hPa and 200 hPa, respectively. The *EASMI* used here was defined as shear vorticity by Wang et al. (2008), i.e. $EASMI = U_{850}$ (110ºE-140ºE, 22.5ºN-32.5ºN) – U_{850} (90ºE-130ºE, 5ºN-15ºN), where U_{850} is boreal summer (JJA) horizontal wind speed at 850 hPa. Shading area shows contrasting phase of the ISMI and EASMI during around 7 ka BP to 4.5 ka BP.

Fig. 5. Spatial patterns (shading color) and associated time series of the EOF modes (principal components, PCs) of the Asian summer (JJA) precipitation for H9K (a: EOF1; b: PC1), H0K (c: EOF1; d: PC1), and HT (e: EOF2; f: PC2). The contour lines in the figures (a, c, e) are correlation square of JJA precipitation with PC1 (a, b) and PC2 (c), respectively. Correlation square above 0.1 is

significant at 95% confidence level.

Fig. 6. Same as Fig. 5 but for the HT JJA precipitation (a: EOF1; b: PC1).

Fig. 7. Map showing subdivisions of the locations of the paleoclimatic proxy records (see Table 2 for cite information and references). The division of regions A-H is after An et al. (2000). The sites of proxy records in the Figure are numbered with 1-94, which match those listed in Table 2. Solid dots in the sub-regions A, B, C, D, E, F, G and H in the Figure indicate proxy records used in An et al. (2000) to divide China into eight sub-regions. Different color of the dots indicates proxy records in different sub-regions.

Fig. 8. Comparison of simulated summer (July, August) precipitation in the HT simulation with moisture indices from the synthesis of multi-proxy records for the Holocene in Regions A, B, C. Shading areas indicate relative wetter period based on proxy data from Zhao et al. (2009a) and Yang et al. (2011).

Fig. 9. Same as Fig. 8 but for Regions D, E, F, G, H. The shading areas indicate relative wetter period based on proxy data from Zhao et al. (2009b) and Zhang et al. (2011).

Fig. 10. Correlation between the Asian summer monsoon intensity (represented by PC1 of HT JJA precipitation, blue line) and ENSO index (represented by DJF Niño 3.4 SST of HT, red line). The proxy record for Holocene ENSO frequency from Laguna Pallcacocha sediment color changes (Moy et al., 2002) is overlapped for a comparison (black line).

Fig. 11. Zonal mean Outgoing Longwave Radiation (OLR) (W/m^2) over region [40ºE-140ºE, 0º-40ºN] for the last 9.5 ka, calculated from experiment HT (shading color). Time series of PC1 of HT (pink line) and proxy record (black line) for the ITCZ (Titanium concentrations (%) in ODP site 1002C from the Cariaco Basin, Haug et al., 2001) are overlapped for a comparison. Relatively strong (S1, S2,..., S8) and weak (W1, W2,..., W8) intervals for summer monsoon strength are marked on the PC1 curve.

Fig. 12. Composite differences in simulated (HT) summer (JJA) sea level pressure (SLP) (pa) (shaded) and 850 hPa wind vectors (m/s) (arrows) between low (9-8 ka BP) and high (2.5-1.5 ka BP) DJF Niño 3.4 SST years.

Fig. 13. Composite differences in simulated (HT) seasonal SST over Pacific in boreal winter (DJF) (a), spring (MAM) (b) and summer (JJA) (c) between low (9-8 ka BP) and high (2.5-1.5 ka BP) DJF Niño 3.4 SST years.

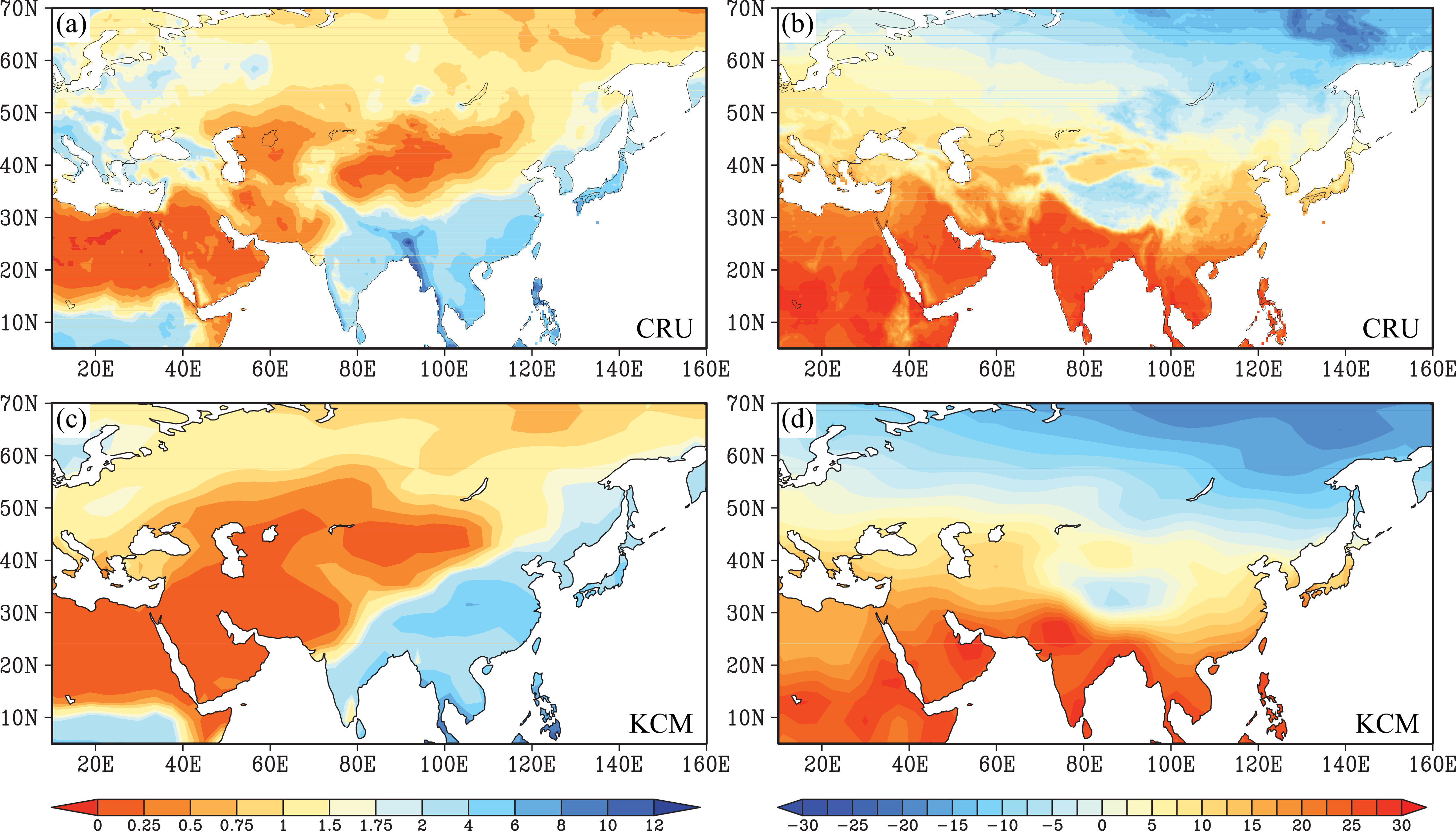

(a)
CRU
(b)
CRU
(c)
KCM
(d)
KCM
70N
60N
50N
40N
30N
20N
10N
20E
40E
60E
80E
100E
120E
140E
160E
0
0.25
0.5
0.75
1
1.5
1.75
2
4
6
8
10
12
−30
−25
−20
−15
−10
−5
0
5
10
15
20
25
30

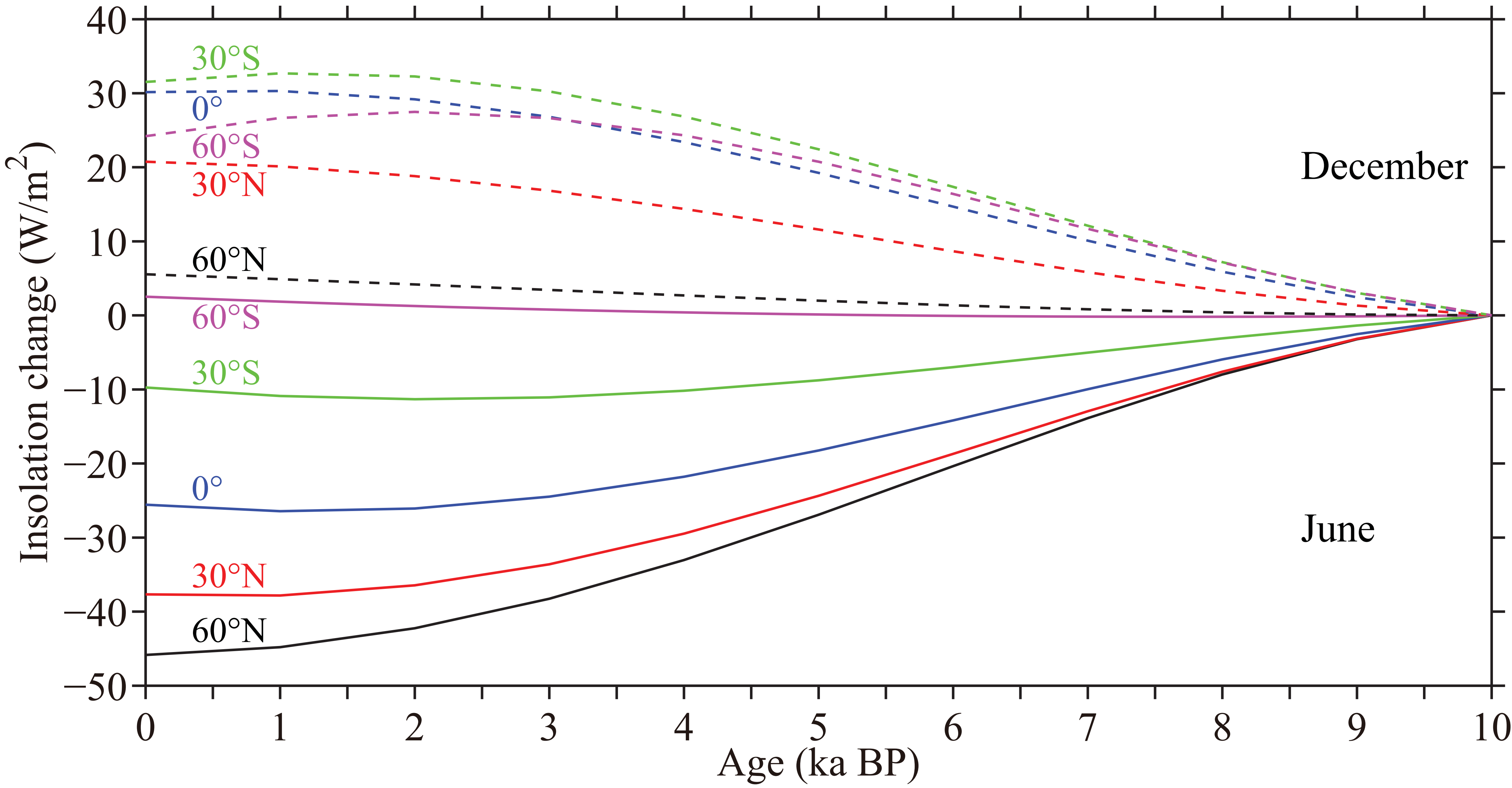

30°S
0°
60°S
30°N
60°N
60°S
30°S
0°
30°N
60°N
December
June
Insolation change (W/m²)
Age (ka BP)
40
30
20
10
0
−10
−20
−30
−40
−50
0
1
2
3
4
5
6
7
8
9
10

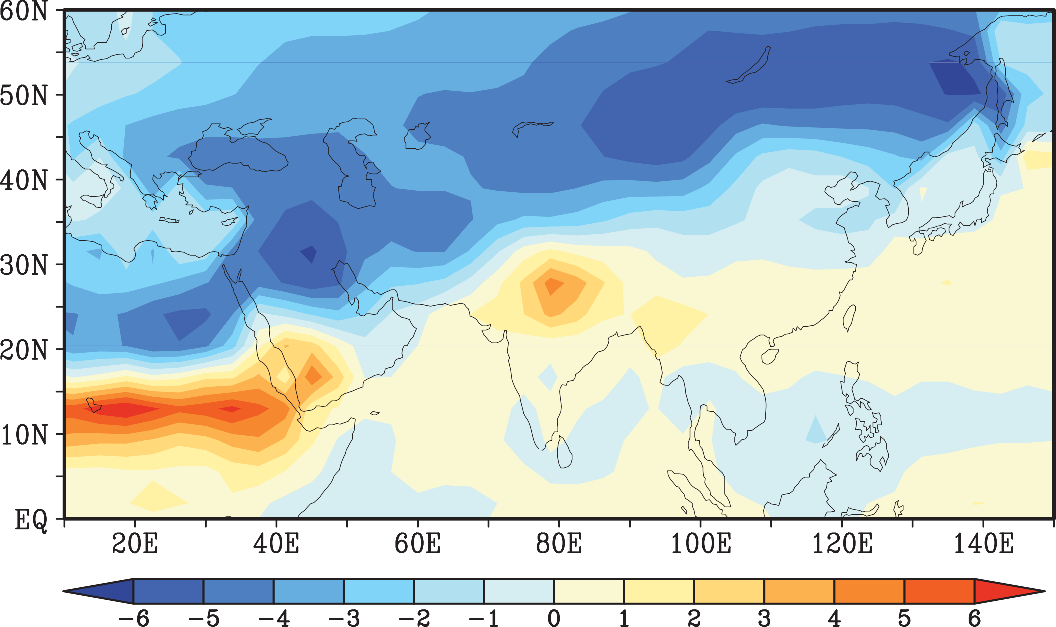
60N
50N
40N
30N
20N
10N
EQ
20E
40E
60E
80E
100E
120E
140E
−6
−5
−4
−3
−2
−1
0
1
2
3
4
5
6

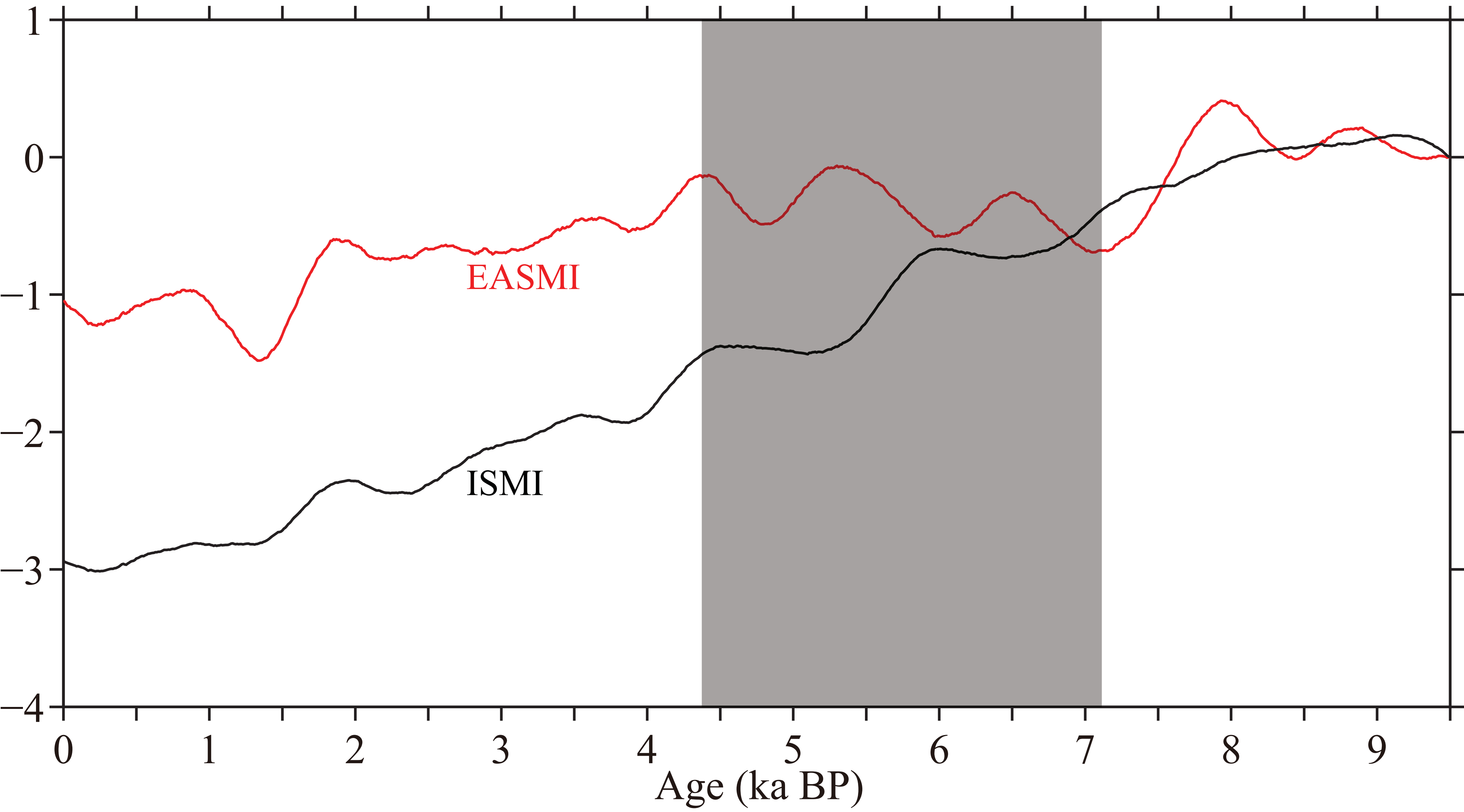
EASMI
ISMI
1
0
−1
−2
−3
−4
0
1
2
3
4
5
6
7
8
9
Age (ka BP)

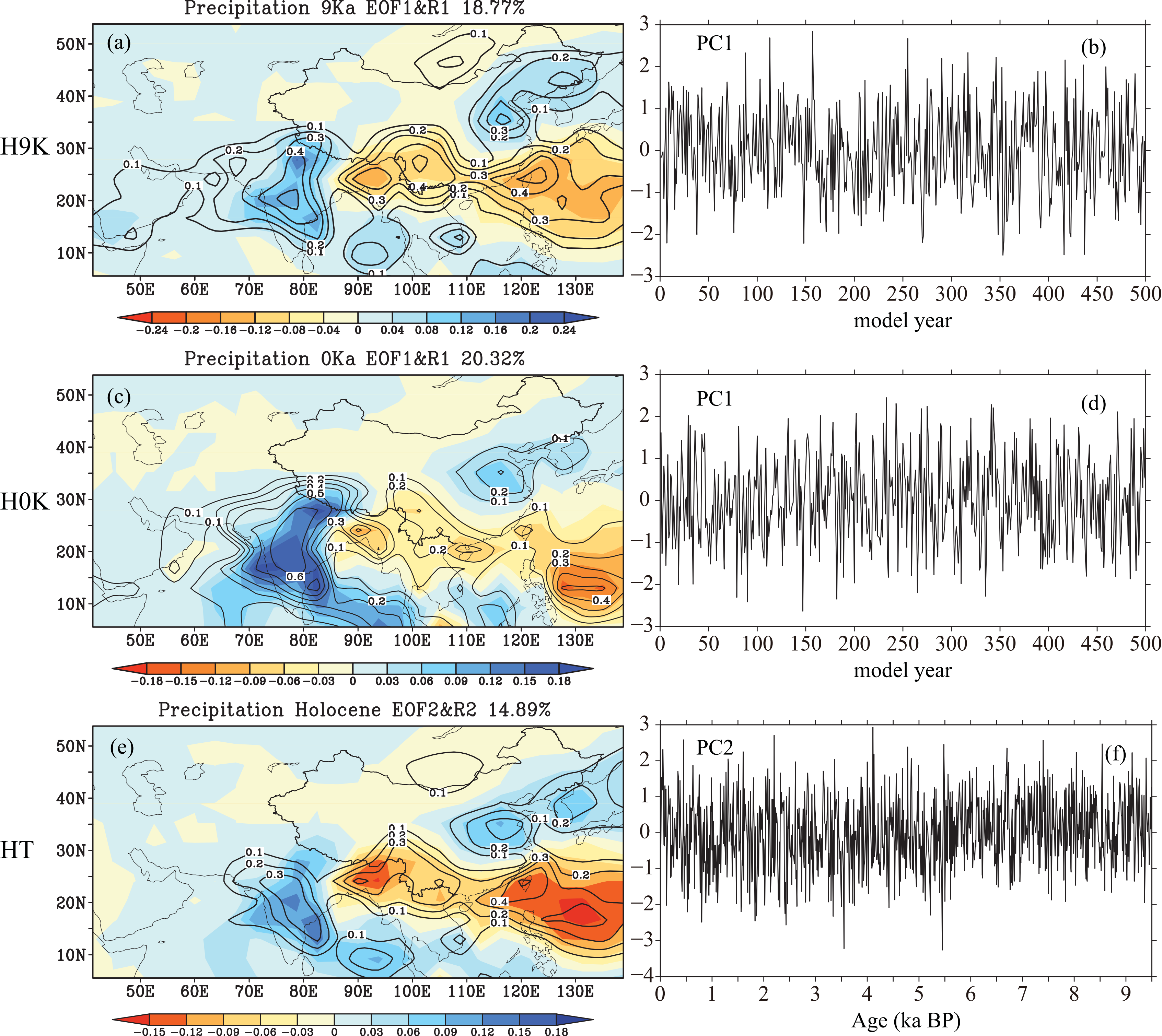
Precipitation 9Ka EOF1&R1 18.77%
(a)
(b)
PC1
H9K
model year
Precipitation 0Ka EOF1&R1 20.32%
(c)
(d)
PC1
H0K
model year
Precipitation Holocene EOF2&R2 14.89%
(e)
(f)
PC2
HT
Age (ka BP)
50E 60E 70E 80E 90E 100E 110E 120E 130E
10N 20N 30N 40N 50N
−0.24 −0.2 −0.16 −0.12 −0.08 −0.04 0 0.04 0.08 0.12 0.16 0.2 0.24
−0.18 −0.15 −0.12 −0.09 −0.06 −0.03 0 0.03 0.06 0.09 0.12 0.15 0.18
−0.15 −0.12 −0.09 −0.06 −0.03 0 0.03 0.06 0.09 0.12 0.15 0.18

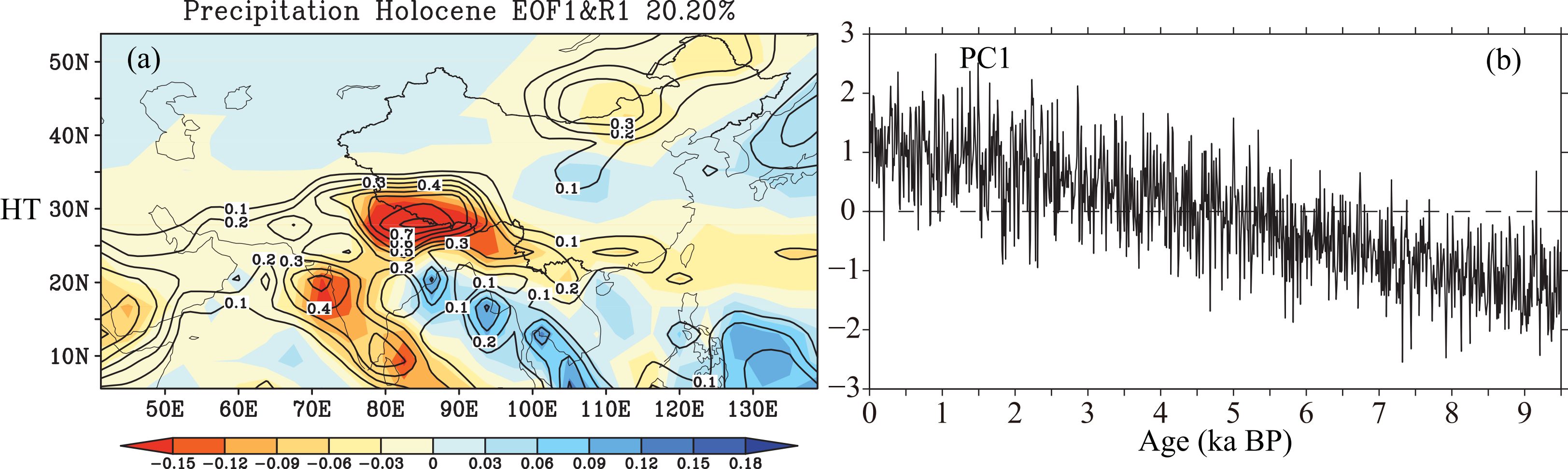

Precipitation Holocene EOF1&R1 20.20%
(a)
HT
50N
40N
30N
20N
10N
50E
60E
70E
80E
90E
100E
110E
120E
130E
−0.15 −0.12 −0.09 −0.06 −0.03 0 0.03 0.06 0.09 0.12 0.15 0.18
PC1
(b)
Age (ka BP)

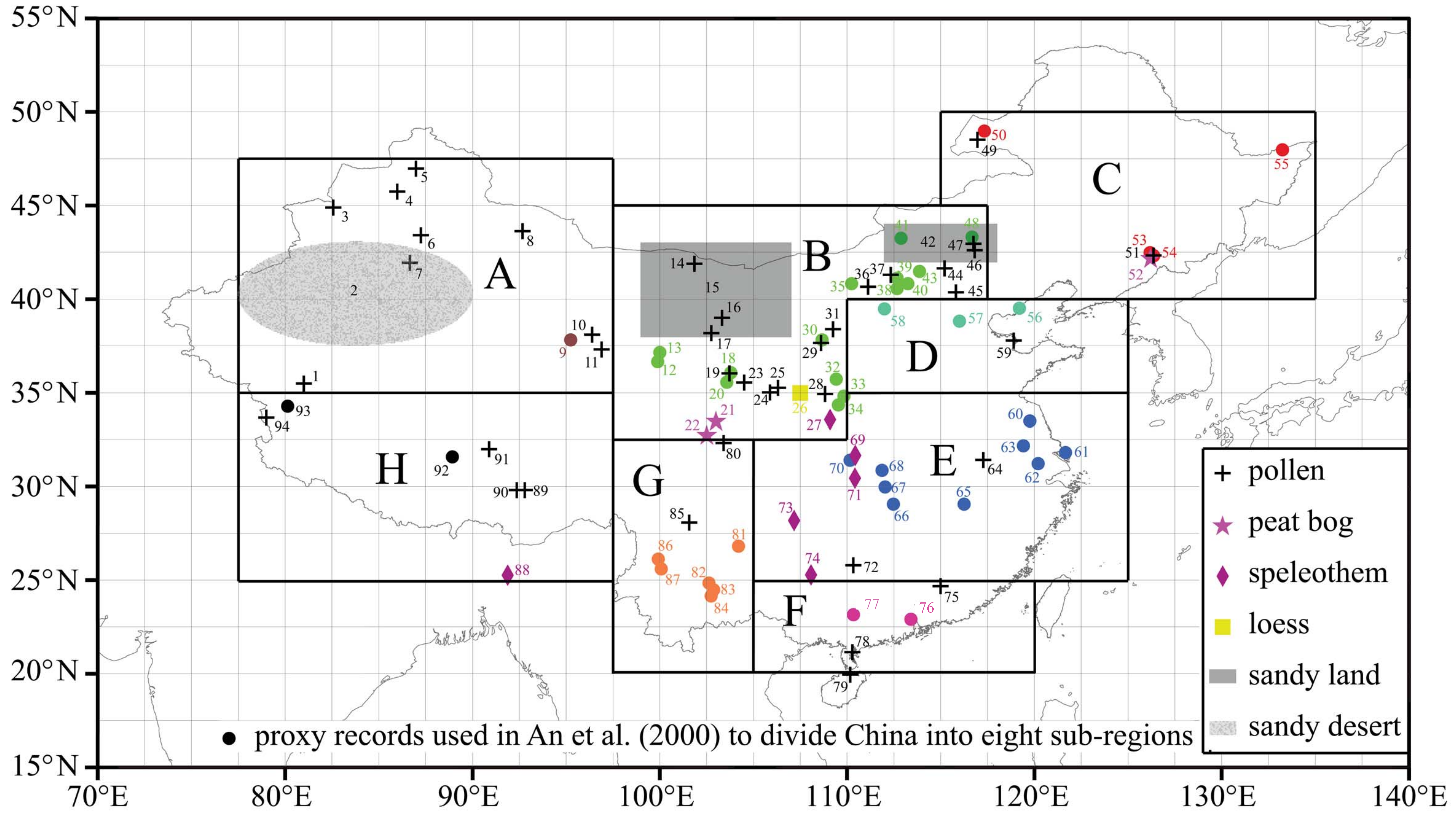

55°N
50°N
45°N
40°N
35°N
30°N
25°N
20°N
15°N
70°E
80°E
90°E
100°E
110°E
120°E
130°E
140°E
A
B
C
D
E
F
G
H
pollen
peat bog
speleothem
loess
sandy land
sandy desert
● proxy records used in An et al. (2000) to divide China into eight sub-regions

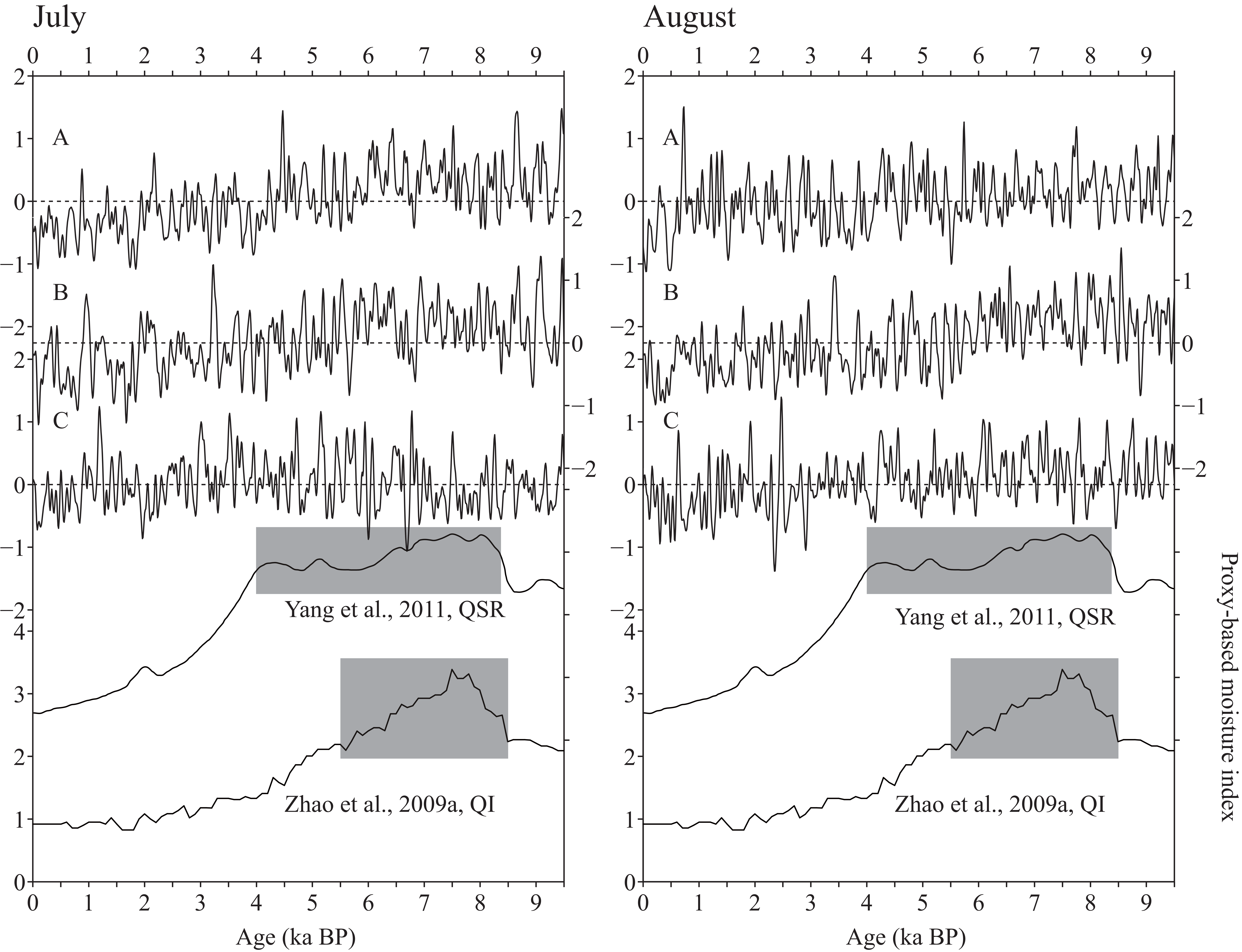

July
August
A
B
C
Yang et al., 2011, QSR
Zhao et al., 2009a, QI
Age (ka BP)
Proxy-based moisture index

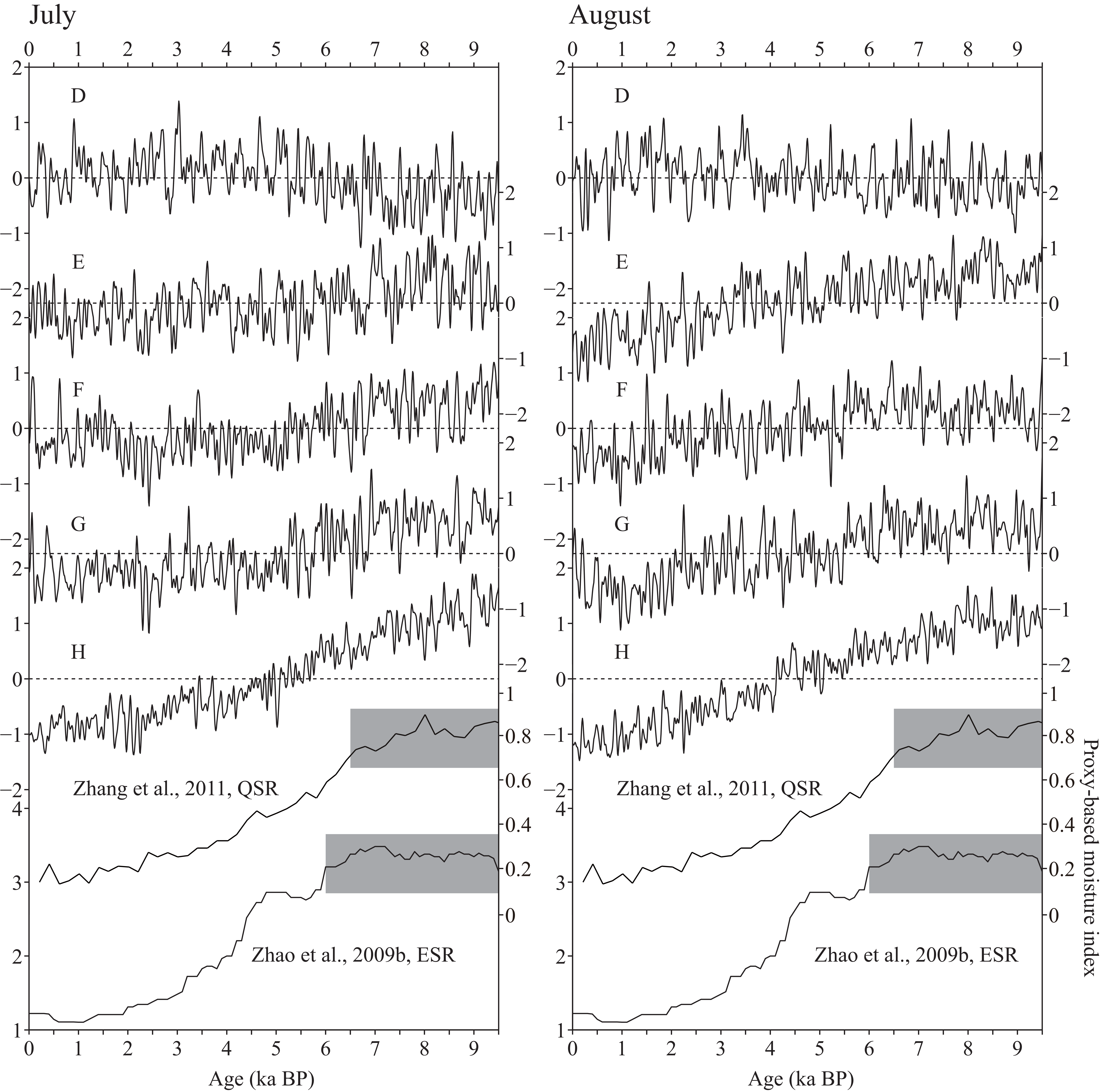

July
August
D
E
F
G
H
Zhang et al., 2011, QSR
Zhao et al., 2009b, ESR
Age (ka BP)
Proxy-based moisture index

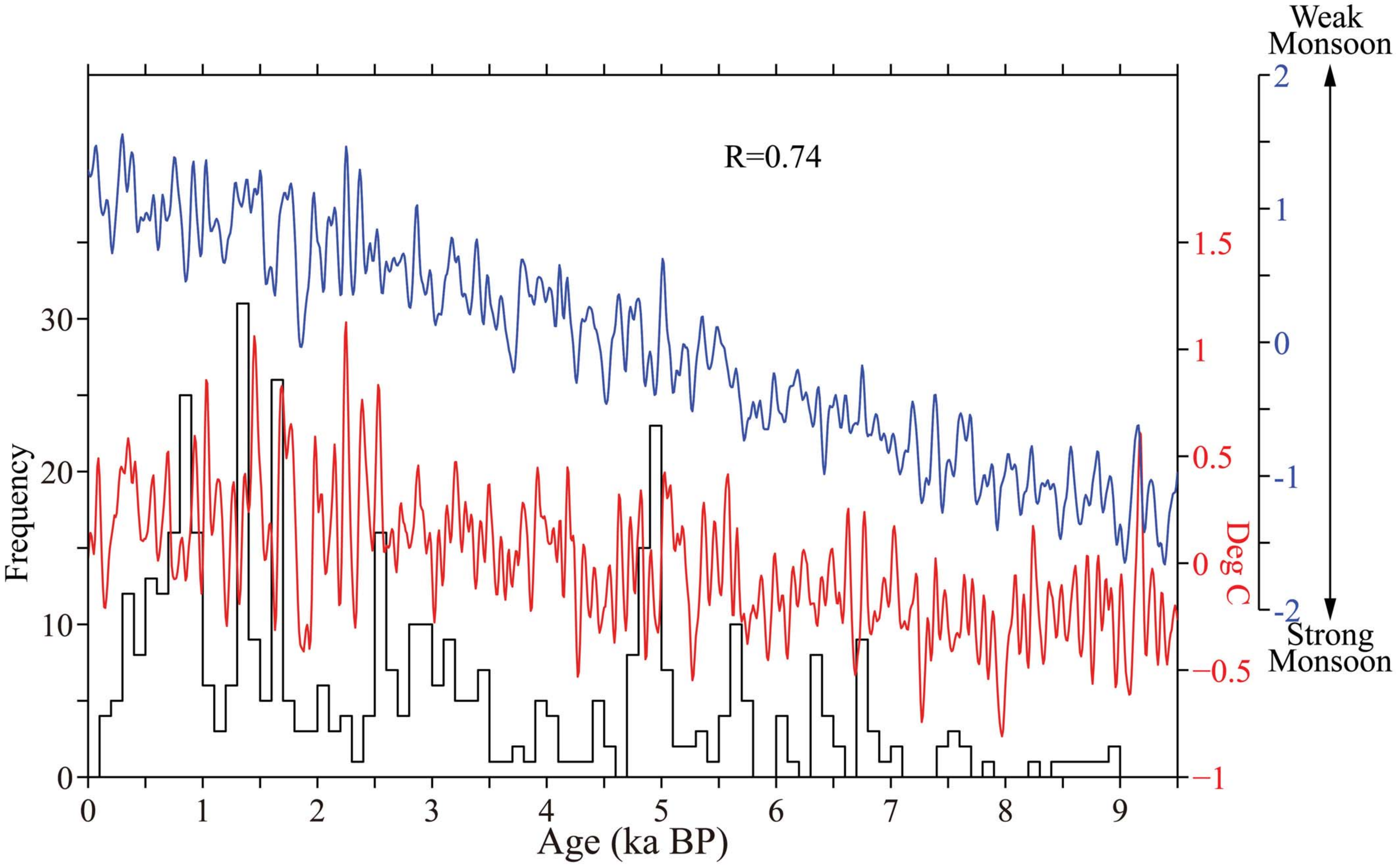

Weak
Monsoon
Strong
Monsoon
R=0.74
Frequency
Deg C
Age (ka BP)
0
10
20
30
−1
−0.5
0
0.5
1
1.5
−2
−1
0
1
2
0
1
2
3
4
5
6
7
8
9

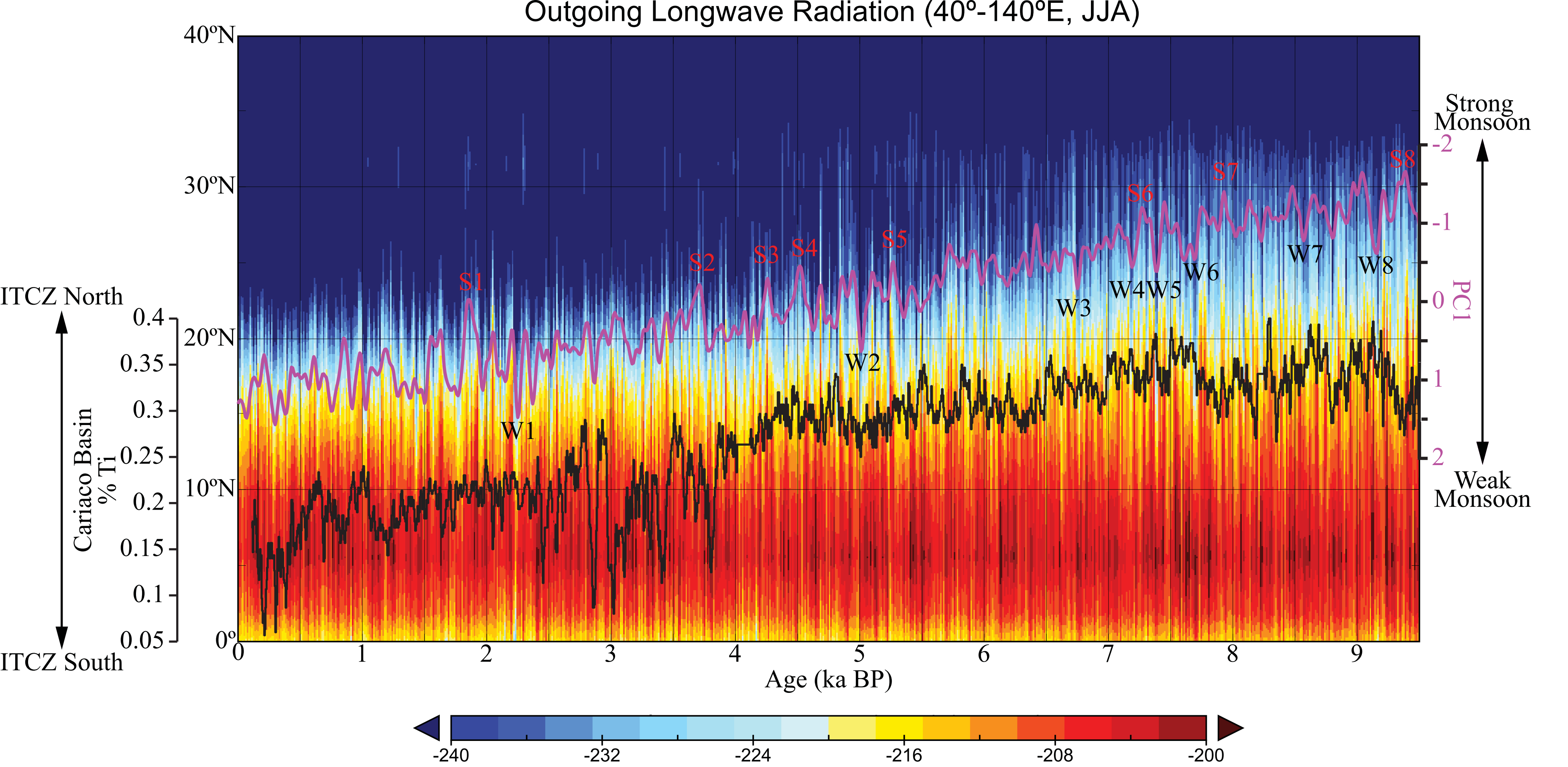

Outgoing Longwave Radiation (40º-140ºE, JJA)
40ºN
30ºN
20ºN
10ºN
0º
ITCZ North
ITCZ South
Cariaco Basin
% Ti
0.4
0.35
0.3
0.25
0.2
0.15
0.1
0.05
Strong Monsoon
Weak Monsoon
PC1
-2
-1
0
1
2
S1
S2
S3
S4
S5
S6
S7
S8
W1
W2
W3
W4W5
W6
W7
W8
0
1
2
3
4
5
6
7
8
9
Age (ka BP)
-240
-232
-224
-216
-208
-200

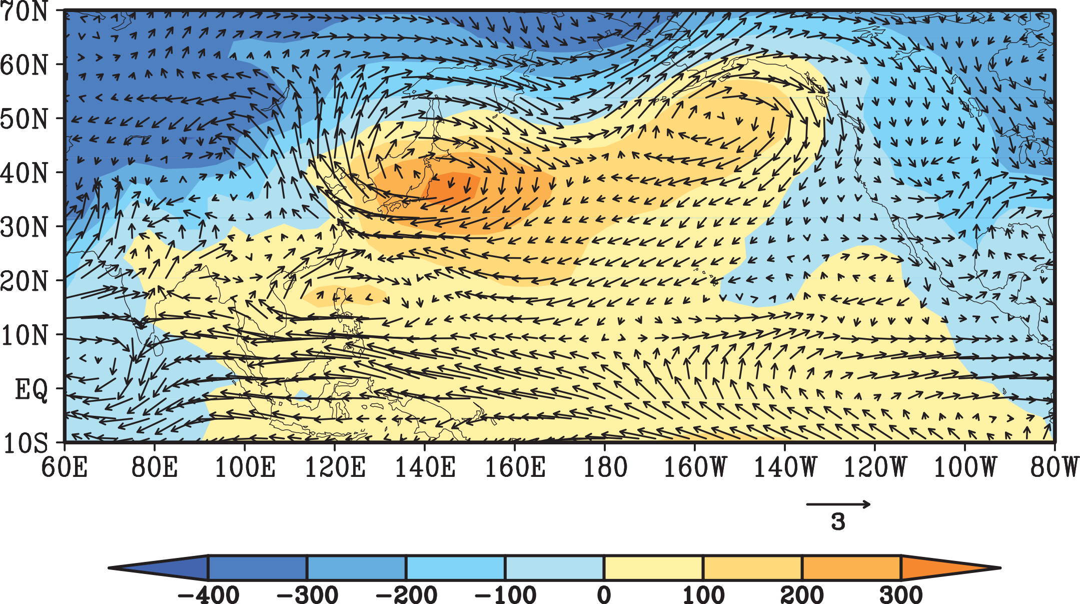
70N
60N
50N
40N
30N
20N
10N
EQ
10S
60E
80E
100E
120E
140E
160E
180
160W
140W
120W
100W
80W
3
−400
−300
−200
−100
0
100
200
300

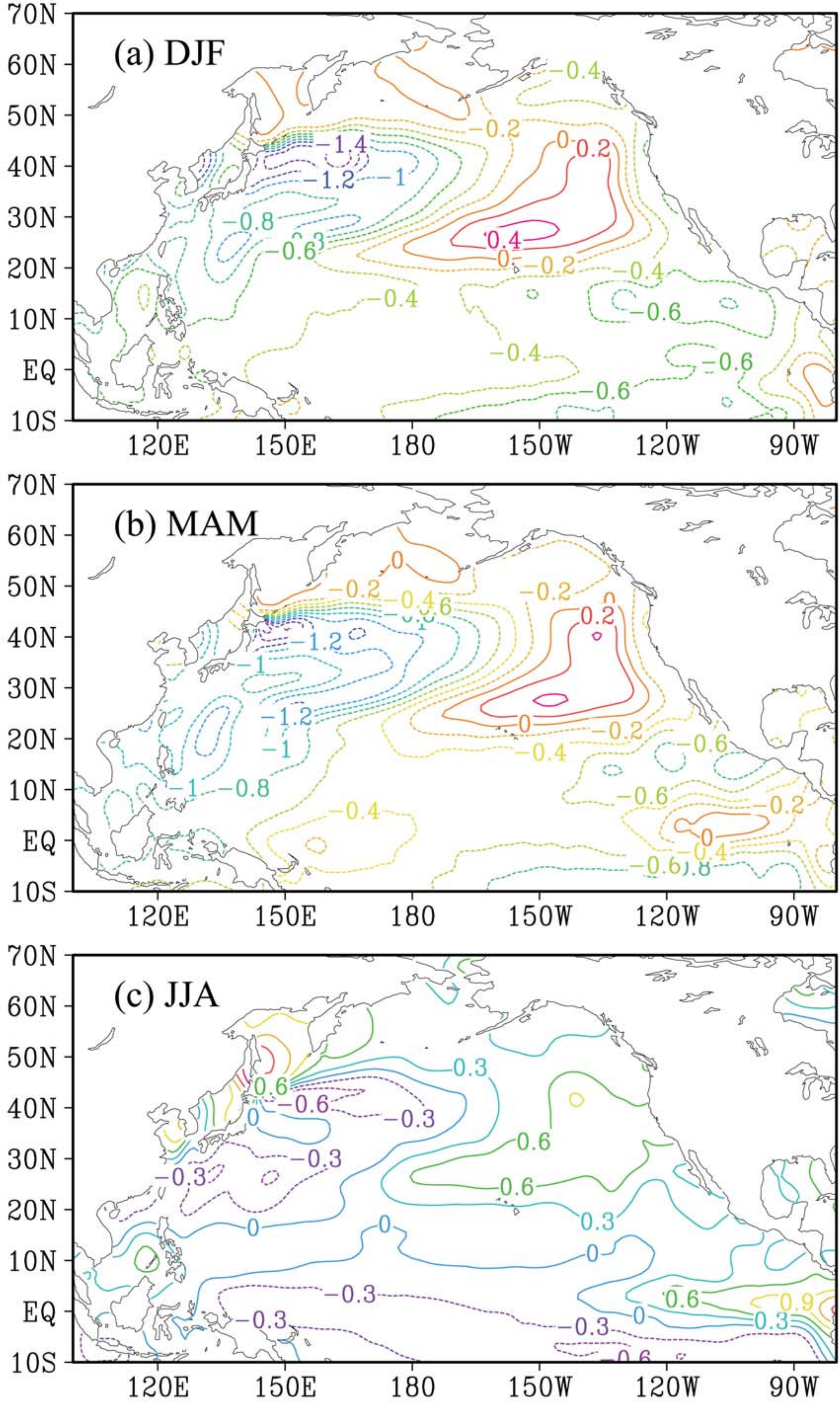

(a) DJF
(b) MAM
(c) JJA
70N
60N
50N
40N
30N
20N
10N
EQ
10S
120E
150E
180
150W
120W
90W
-1.4
-1.2
-1
-0.8
-0.6
-0.4
-0.2
0
0.2
0.4
0.3
0.6
0.9
-0.3
-0.6

Supplementary Information

Supplementary Figure captions

Fig. S1. Comparison of spring (March-April-May, MAM) mean precipitation (mm/day) (a, c) and MAM mean surface temperature (ºC) (b, d) from the Climate Research Unit TS 2.1 dataset for 1901-1930 (a, b) and KCM pre-industrial simulation (c, d).

Fig. S2. Comparison of summer (June-July-August, JJA) mean precipitation (mm/day) (a, c) and JJA mean surface temperature (ºC) (b, d) from the Climate Research Unit TS 2.1 dataset for 1901-1930 (a, b) and KCM pre-industrial simulation (c, d).

Fig. S3. Comparison of autumn (September-October-November, SON) mean precipitation (mm/day) (a, c) and SON mean surface temperature (ºC) (b, d) from the Climate Research Unit TS 2.1 dataset for 1901-1930 (a, b) and KCM pre-industrial simulation (c, d).

Fig. S4. Comparison of winter (December-January-February, DJF) mean precipitation (mm/day) (a, c) and DJF mean surface temperature (ºC) (b, d) from the Climate Research Unit TS 2.1 dataset for 1901-1930 (a, b) and KCM pre-industrial simulation (c, d).

Fig. S5. Comparison of simulated trends of last 6 ka for global zonal-mean JJA precipitation (PREC) and surface air temperature (SAT) by KCM (Liya_Jin, brown line) with other models (referenced from the INTERDYNAMIK 2010 Status Seminar, Bremen, Germany, http://www.geo.uni-bremen.de/interdynamik/)

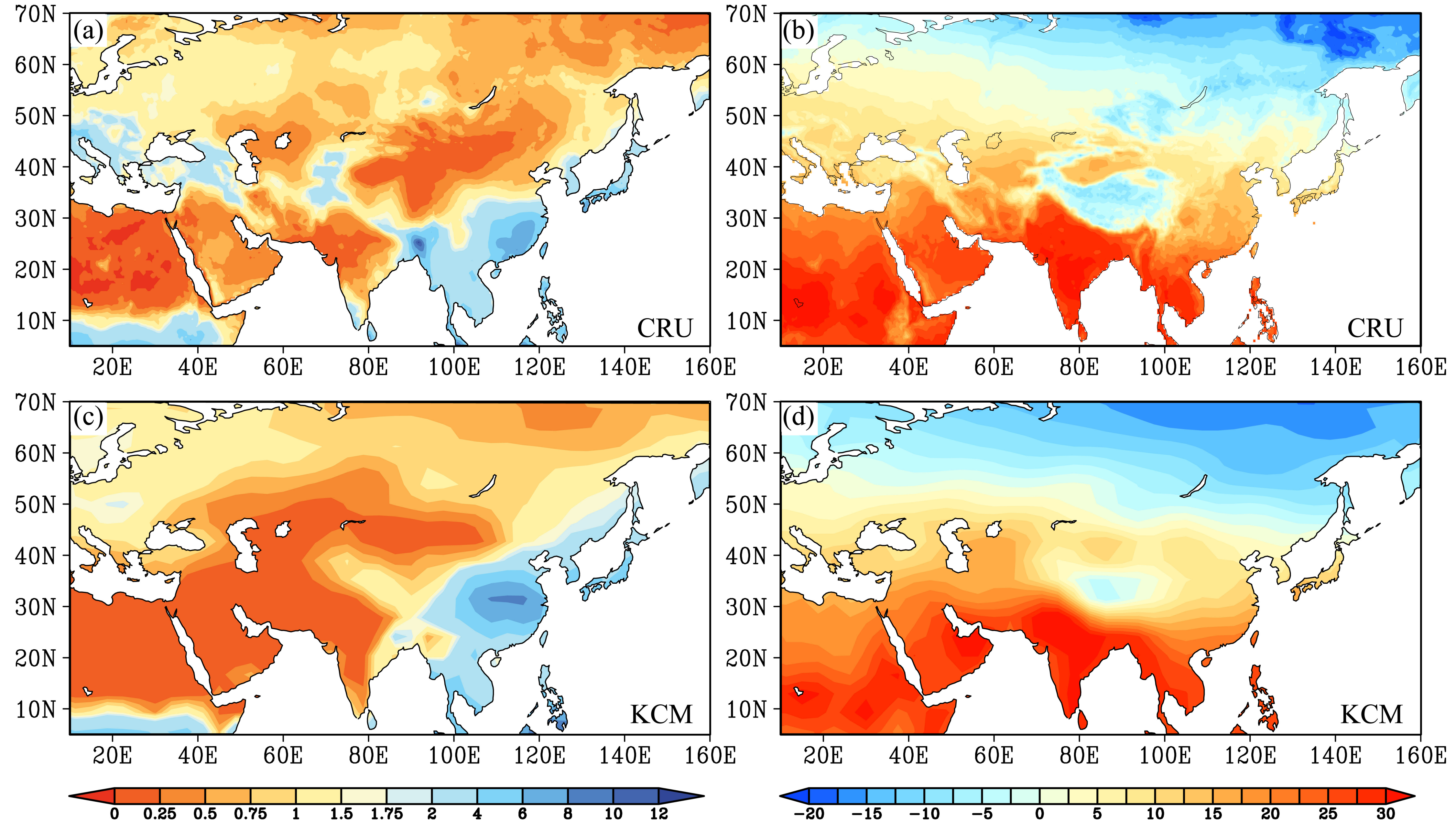
(a)
CRU
(b)
CRU
(c)
KCM
(d)
KCM
70N
60N
50N
40N
30N
20N
10N
20E
40E
60E
80E
100E
120E
140E
160E
0
0.25
0.5
0.75
1
1.5
1.75
2
4
6
8
10
12
−20
−15
−10
−5
0
5
10
15
20
25
30

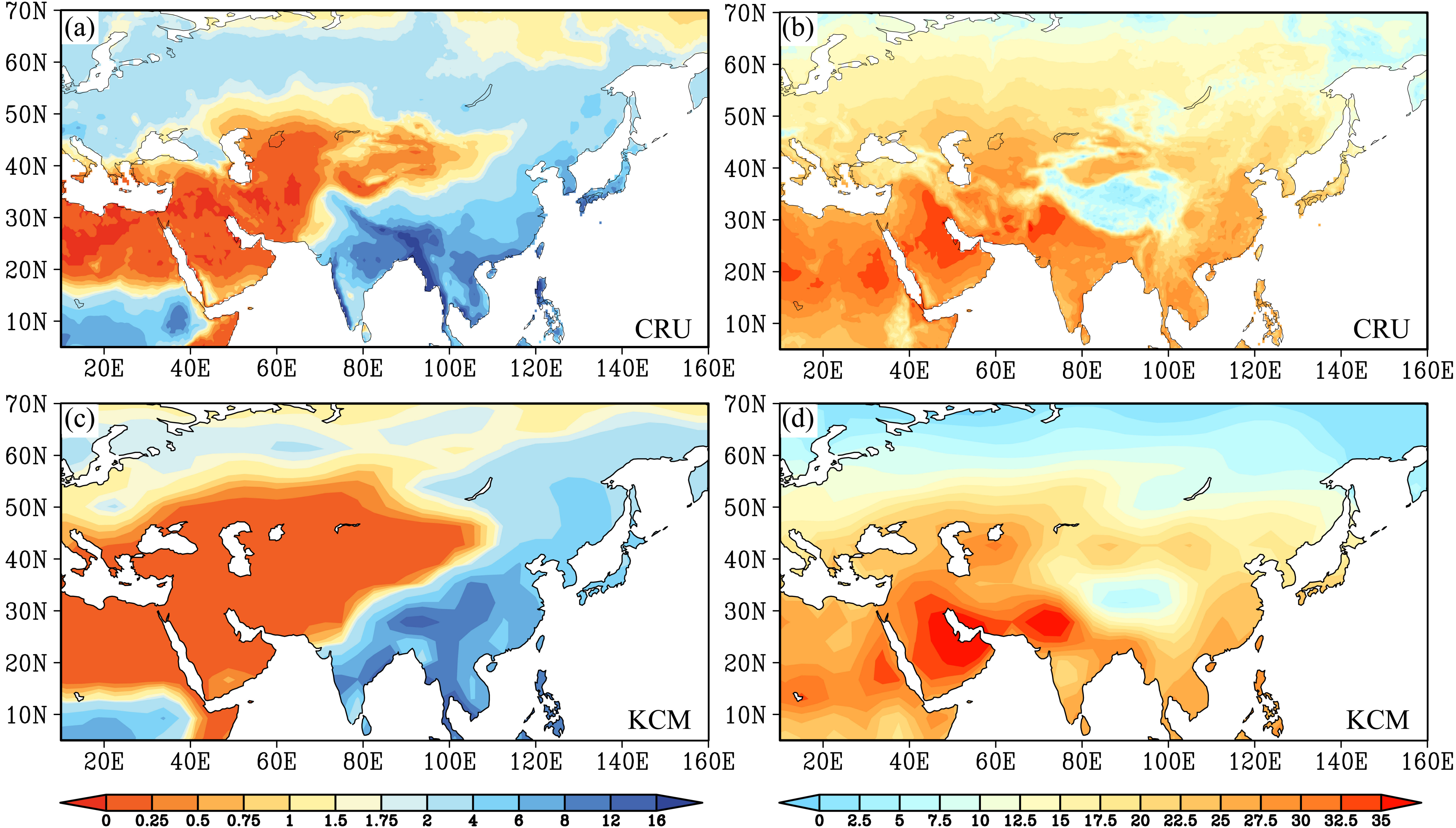
(a)
CRU
(b)
CRU
(c)
KCM
(d)
KCM
70N
60N
50N
40N
30N
20N
10N
20E
40E
60E
80E
100E
120E
140E
160E
0 0.25 0.5 0.75 1 1.5 1.75 2 4 6 8 12 16
0 2.5 5 7.5 10 12.5 15 17.5 20 22.5 25 27.5 30 32.5 35

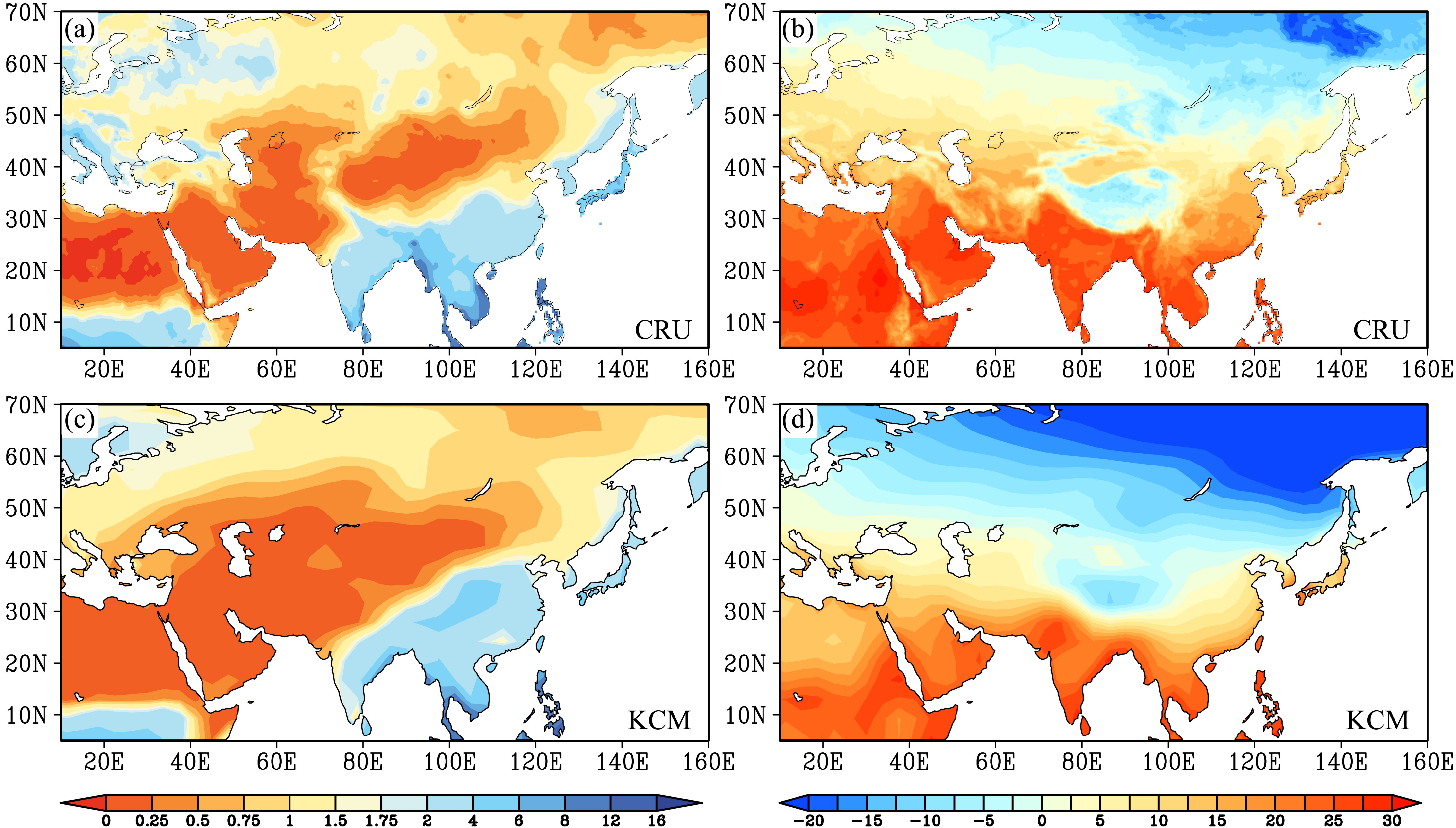

(a)
CRU
(b)
CRU
(c)
KCM
(d)
KCM
70N
60N
50N
40N
30N
20N
10N
20E
40E
60E
80E
100E
120E
140E
160E
0
0.25
0.5
0.75
1
1.5
1.75
2
4
6
8
12
16
−20
−15
−10
−5
0
5
10
15
20
25
30

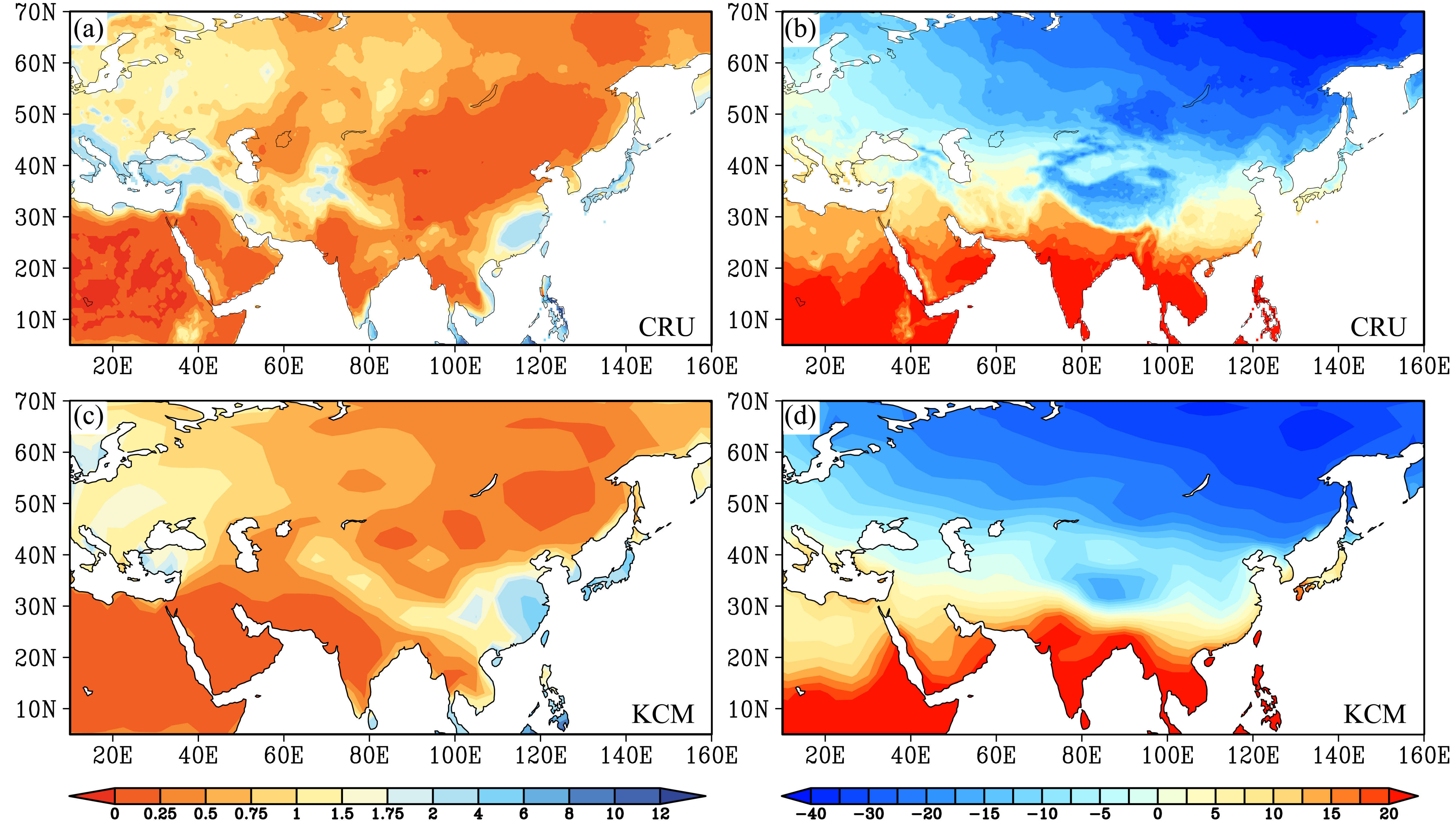

(a)
CRU
(b)
CRU
(c)
KCM
(d)
KCM
70N
60N
50N
40N
30N
20N
10N
20E
40E
60E
80E
100E
120E
140E
160E
0
0.25
0.5
0.75
1
1.5
1.75
2
4
6
8
10
12
−40
−30
−20
−15
−10
−5
0
5
10
15
20

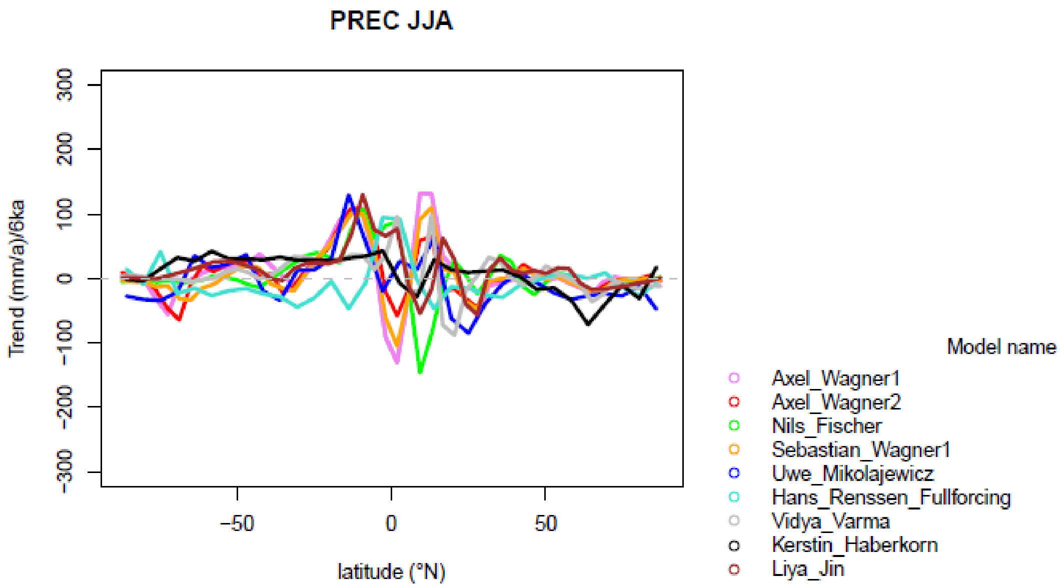

(a) Summer (June-July-August, JJA) precipitation

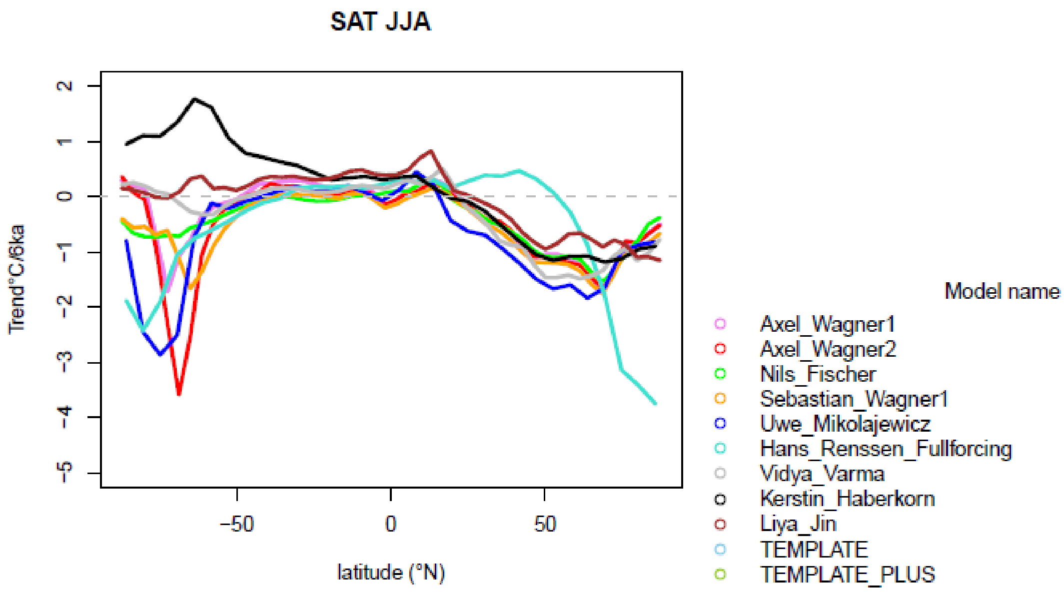

(b) Summer (JJA) surface air temperature

Fig. S5. Comparison of simulated trends of last 6 ka for zonal-mean summer (JJA) (a) precipitation (PREC) and surface air temperature (SAT) (b) by KCM (Liya_Jin, brown line) with other models (referenced from the INTERDYNAMIK 2010 Status Seminar, Bremen, Germany, http://www.geo.uni-bremen.de/interdynamik/)